





### Particle granular temperature in gas fluidized beds

G.D. Cody a, D.J. Goldfarb a, G.V. Storch, Jr a, A.N. Norris b

<sup>a</sup> Exxon Corporate Research Laboratory, Annandale, NJ 08801, USA
<sup>b</sup> Department of Mechanical and Aerospace Engineering, Rutgers University, Piscataway, NJ 08855 USA

Received 23 June 1995; revised 8 December 1995

#### Abstract

In this paper we introduce and validate a novel non-intrusive probe of the average kinetic energy, or granular temperature, of the particles at the wall of a gas fluidized bed. We present data on the granular temperature of monodispersed glass spheres which span region B, and extend into region A, of the Geldart powder classification. The underlying physics of the measurement is the acoustic shot noise excitation of the surface of the fluid bed vessel by random particle impact. Quantitative determination of the average particle granular temperature is obtained through independent measurement of the wall transfer function determining the coupling between the acoustic shot noise excitation at one location and the response of an accelerometer at another location. We validate the concept and calibration of this acoustic shot noise probe in the frequency range 10-20 kHz, through a comprehensive series of laboratory measurements with gasses and cylinders of significantly different acoustic properties. We demonstrate its utility by presenting the first data on the dependence of the granular temperature on gas flow and particle diameter and make the first observation of a change in the character of the fluidization transition from first order (hysteretic and discontinuous) to second order (reversible and continuous) for Geldart B glass spheres as the A/B boundary is approached. We observe a striking difference in the dependence of the granular temperature on gas flow between Geldart B and A glass spheres, that suggests a fundamental difference in particle dynamics between spheres in the two Geldart regimes. Finally we use the vibrational probe to study the time dependence of the granular temperature under bed collapse conditions when fluidizing gas is withdrawn rapidly from the system. We show an exponential time dependence with a time constant of the order of 100 ms, and demonstrate the consistency of this result with a Langevin equation for the sphere velocity with a time constant derived from the sphere fluctuation velocity and a collisional coefficient of restitution of 0.9. From these results for the granular temperature and a kinetic model for a dense granular gas, we present estimates for the inertial pressure, velocity of sound, viscosity, and diffusion constant of the dense phase of a gas fluidized bed as a function of particle diameter and gas superficial velocity. The implication of these results for current models of gas fluidized beds, and the fundamental basis of the Geldart classification is discussed.

Keywords: Particle granular temperature; Gas fluidized beds; Kinetic energy; Acoustic shot noise; Particle dynamics; Geldart classification

### 1. Introduction

If the gas flow through a cylinder confining a bed of packed particles is increased, the pressure drop across the bed increases linearly until its magnitude is equal to the weight of the bed. At this critical flow velocity the particle/gas system makes a transition to a fluidized state which exhibits many of the properties of a liquid [1]. As gas flow is increased above the critical velocity, the pressure drop across the bed remains constant. The bed height initially increases at the same critical velocity, and continues to change continuously above it. Gas-rich bubbles appear as a second phase within the fluidized bed and their arrival at the surface gives the bed the appearance of boiling. Fluidized beds play an important role in continuous petroleum, chemical, and combustion processes that are based on particle gas interactions [2].

Although there have been important advances in understanding fluid bed phenomena, for example, modeling gas and particle flow through individual bubbles [3] and modeling the instability of fluidized beds [4], a fundamental, first principles theory of the hydrodynamics of these dense two-phase systems has yet to be achieved. However, the remarkable and continuing increase in computational power is encouraging with respect to advances in theory [5].

Less encouraging is the rate of advance in experimental probes of fluidized beds. As summarized in a recent review: "During the 50 or so years since the widespread introduction of fluidized beds many experimental methods have been devised to study their internal workings...... There remains, however a need for monitoring equipment that can be used reliably on an industrial scale under hostile conditions of atmosphere, temperature and pressure. Some of the probes

described above are suited to this type of operation but question remains about the effect they induce on the local hydrodynamics. Non-invasive techniques, such as radiation attenuation and tomographic imaging, are generally to be preferred but to date these suffer from problems of data interpretation and from the sometimes low level of discrimination they are able to offer'' [6]. It is hoped that the subject of this paper, a novel and non-invasive acoustic probe of the particle granular temperature at the wall of fluidized beds, will meet the need to supply critical experimental insights and validation for recent theoretical models, as well as avoid the indicated pitfalls.

Due to the complexity of the dynamics of the particle gas system and, perhaps the absence of appropriate, non-invasive experimental probes, the science of fluidization continues to be dominated by useful empirical correlations based on well-chosen dimensionless groups, rather than on fundamental theory. Despite the evident technological success of this approach, there remain surprising gaps. Batchelor noted in 1988, almost 50 years after the first commercial application of fluidized beds in catalytic cracking, that while "there is a general belief that a uniform fluidized bed may be unstable, the underlying physical mechanisms are not yet clear" [7].

There is a growing theoretical [8,9] and experimental [10–12] interest in the study of granular flow, in which fluid forces are neglected. This research area has generated new insights on the interaction between inertial and frictional forces in the mechanics of flowing particles and introduced physical concepts that may contribute to a fundamental theory of fluidized beds. Both particle/particle and particle/fluid forces are critical in the behavior of fluid beds, but some granular flow concepts can be employed to simplify the complexity and multiplicity of equations describing the dynamics of particles, gas, and their interactions [13].

Particularly relevant to the present paper are recent theories that isolate the generation, flow, and dissipation of the average particle kinetic energy or granular temperature as explicit terms in the particle/fluid equations of motion [14,15]. The concept of the granular temperature assists in closing numerical computations. It can also supply insights into the study of transport phenomena in such complex systems as, for example, sound propagation, diffusivity and viscosity of dusty gasses, developed from the kinetic theory of dense gasses [14–17]. It can also serve as a starting point for the study of wall erosion phenomena [18–20]. Unfortunately, despite indications of increasing theoretical interest in the granular temperature concept [5], there are few, if any, reports of the measurement of the granular temperature.

In this paper we introduce acoustic shot noise, as the fundamental physical mechanism underlying a novel non-intrusive, quantitative probe of the average granular temperature at the wall of a gas fluidized bed. The new probe is considerably more sensitive than the traditional probes of fluidization, and, as will be seen, has supplied a number of new insights:

- (i) the first evidence for a change in the order of the fluidization transition for glass spheres as sphere diameter is reduced;
- (ii) the discovery that well above minimum fluidization, the average granular temperature is inversely proportional to the square of the particle diameter and directly proportional to the square of the gas superficial velocity; and
- (iii) the discovery that the dependence of the granular temperature on gas superficial velocity exhibits systematic differences between glass spheres that are in the Geldart A and Geldart B fluidization classifications [21–23] and that a fundamental feature of so-called aeratable Geldart A particles is a significantly enhanced granular temperature just above minimum fluidization.

Finally, we show the utility of the new probe by the first measurements of the time dependence of the granular temperature during bed collapse experiments [24,25] where the fluidizing gas is removed rapidly from the system. We find that the granular temperature decays exponentially, and from the exponential time constant we have obtained the first insitu measurement of the energy loss per collision (coefficient of restitution) of the collision of glass spheres within a gas fluidized bed.

### 2. Granular temperature

We define a particle distribution function with respect to velocity, f(c), where f(c(r,t))dc is the probability of finding a particle with the vector velocity c at location r at time t. For elastic particle collisions f(c(r,t))dc is given by the Maxwellian velocity distribution which is a steady-state solution to the Boltzman equation [26,27]. For the macroscopic particles found in a fluidized bed, particle collisions are inelastic and a Maxwellian function is not a solution to the Boltzman equation, but can serve as a starting point for a perturbation expansion [15,28]. If we denote the particle velocity as c(r,t), its ensemble average defines the particle drift velocity, V(r,t), at the location r, where  $V(r,t) \equiv$  $\langle c(r,t) \rangle$ . V(r,t) is an obvious visual feature of a fluidized bed since it describes the downward convective flow of spheres at the wall. The sphere fluctuation velocity, w(r,t) =c(r,t) - V(r,t), is much too rapid to be a visual feature, but is the major contribution to the granular temperature.

The granular temperature,  $T^*$ , defined as the ensemble average of the squared fluctuation velocity, is given by  $3T^* \equiv \langle w(r,t)^2 \rangle = \langle c(r,t)^2 \rangle - [V(r,t)]^2$ . For fluidized beds  $[V(r,t)]^2 \ll \langle c^2 \rangle$ , and hence the mean square of the sphere velocity,  $\langle c^2 \rangle$ , dominates the granular temperature,  $T^*$ . With the assumptions of spatial uniformity and isotropy,  $T^*$  can be expressed by one component of  $\langle c^2 \rangle$ . For later convenience, we choose the velocity component normal to the wall,  $v_n(r,t)$ , and thus write  $T^* \equiv (\langle w(r,t)^2 \rangle / 3) \approx \langle v_n(r,t)^2 \rangle \equiv v_n^2$ .

The concept of a granular temperature exploits the analogy between the random motion of a dense dusty gas of particles in a fluidized bed and the thermal motion of molecules. In the kinetic theory of gasses the thermal temperature T results from imposing equipartition of energy on the Maxwellian distribution. In contrast,  $T^*$ , is not a thermodynamic property but is a steady state constant determined by the complex interaction between the viscous and inertial forces exerted on a particle by its local gas and particle environment. Since particle collisions within a fluid bed are inelastic, the granular temperature can only be a dynamic constant through the power supplied to the bed by the fluidizing gas. Furthermore, in contrast to molecular gasses where the mean free path is many orders of magnitude greater than the particle diameter, dusty gasses exhibit inter-particle separations and particle mean free paths which are of the same order as the particle diameter.

Despite these important distinctions, the granular temperature concept has been described by Campbell [29] as the "single most important key to understanding the behavior of rapid granular flows". It plays an increasingly significant role in recent theoretical work on the properties of fluidized beds and transfer lines, and on general granular flow.

There are few reported measurements of the granular temperature. To quote again from Batchelor [7], "it should be possible to make measurements of...the non-dimensional mean square particle velocity fluctuation in a uniform fluidized bed...[but] there are few published data". Particle velocity data is available from laser Doppler velocity measurements, but the focus has been on mean flow velocity, V(r,t), in dilute systems [30,31]. Comparable data on  $T^*$  is lacking. Other optical techniques such as optical fiber correlators appear to have been again restricted to measurements of V(r,t) [32,33]. There continues to be a surprising gap between the growing theoretical importance of the granular temperature and its measurement.

### 3. Acoustic shot noise

The acoustic shot noise probe of the granular temperature is based on a quantitative analysis of the response of the wall of a vessel to random particle impact. We utilize power spectral analysis for the derivation, in particular the fundamental theorem of Wiener and Khintchine which states that, for stationary random functions, the power spectrum of a random function is the Fourier transform of its autocorrelation function [34,35]. Given the novelty of our experimental approach, we focus on the fundamental physics of acoustic shot noise, its relation to the average particle fluctuation velocity at the wall of a fluidized bed, and its experimental validation. Mathematical rigor has not been ignored in this paper, but it has not been emphasized. We believe that a more rigorous mathematical analysis would not result in changes in the magnitudes of derived physical quantities by a significant factor.

For particles with mass m colliding with the wall with normal velocity,  $v_n$ , the momentum exchange with the wall

due to elastic particle impact is  $\Delta p = (2mv_p)$ . The power spectrum of the particle force depends not just on  $\Delta p$ , but also on the duration of the collision, or impact time,  $\Omega$ , which determines its frequency content. Landau and Lifshitz [36] derive the magnitude of  $\Omega$  for the case of a spherical particle of diameter D, impacting a flat surface of the same material with normal velocity  $v_n$ . Using their analysis, we find, for particle sizes from 50 to 500  $\mu$ m, and particle velocities of 1–100 cm/s, a Fourier transform of the particle impact force of constant magnitude below 300 kHz. In the language of power spectrum analysis, the power spectrum due to random particle impact of these particles is white noise for frequencies below 300 kHz. This is a simplifying, but not critical, assumption in the mathematics. It is exact for the present experiments since all the vibrational data are restricted by accelerometer and signal processing constraints to the frequency range 0-25.6 kHz. In that frequency range, we can accurately represent the time dependent force of one particle by a Dirac delta function,  $\delta(t)$ . For random elastic particle impacts on an area  $\Delta A$  of the internal wall of a cylinder, the resultant force F(t) in this frequency range is thus given by

$$F(t) = \sum_{i=1}^{n} 2mv_n \delta(t - t_i)$$
 (1)

We further assume that the arrival times of the particles,  $t_i$ , are randomly and uniformly distributed such that there are  $\nu T$  impacts in the time interval T, where  $\nu$  is the mean rate of arrival of the particles on the area  $\Delta A$ . The time average of Eq. (1) is then given by  $\langle F(t) \rangle = 2 m v_n \nu$ . This relationship should be familiar as the starting point for the calculation of the pressure exerted on the wall of a vessel by the impact of the molecules in a gas. The frequency dependent force of random particle impact, which is the source of acoustic shot noise, will be obtained from the power spectrum of F(t).

The power spectrum corresponding to Eq. (1) is given by  $S_F(f) = [1/W] < F(f)^2 > \text{ where } F(f) \text{ denotes the Fourier transform of } F(t), \text{ the brackets } <> \text{ indicate a time and ensemble average over the arrival time of the particles, and } W is the time interval over which the autocorrelation function of <math>F(t)$  is averaged. If we assume a uniform distribution function of the random arrival times, the power spectrum of the force due to random particle impact on the area,  $\Delta A$ , of the wall of the vessel at  $R = R_i$ , can be easily shown to be given by:

$$S_{\rm F}(f,R_{\rm i}) = (2mv_{\rm n})^2 \nu = (4m\rho_{\rm m}v_{\rm n}^3\Delta A)|_{R_{\rm i}}$$
 (2)

where we have expressed the mean rate of arrival of the particles,  $\nu$ , by the dilute gas expression,  $\nu = \rho_b \nu_n \Delta A$ . The quantity  $\rho_m = m\rho_b$  is the bed mass density and  $\rho_b$  is the volume number density of particles in the bed. The particles in a fluid bed are far from dilute, but the average arrival rate can be shown, within a factor of the order of unity which depends on the roughness of the wall relative to the particle size, to be given by  $\nu = \rho_b \nu_n \Delta A$ .

Eq. (2) is the power spectrum for acoustic shot noise which at acoustic frequencies is a white noise source exhibiting no explicit frequency dependence. Eq. (2) is the starting point for determining quantitatively the sound generated by hail on a roof or the vibrational energy imparted to the wall of a fluidized bed by random particle impact. Gas molecules have small masses and large velocities, and their acoustic shot noise contribution to dynamic pressure in the acoustic frequency range is 10 orders of magnitude below their contributions to the static pressure, and only measured with great difficulty. However, if the human ear were considerably more sensitive, acoustic shot noise due to molecular impact on the ear drum would contribute a constant background hiss to our hearing. For the large masses of particles within fluidized beds conditions are different. The dynamic pressure noise in a fluidized bed can be shown to be only about an order of magnitude less than the particle contribution to static pressure [37], and easily measured with readily available instrumentation. Despite the simplicity of the derivation of Eq. (2), it does not appear to be as widely known as the mathematically equivalent shot noise power spectrum produced by the random arrival times of electrons in electronic devices [34].

Acoustic shot noise is frequency independent in the experimental frequency range considered in this paper. However, the response of the cylinder to this random force can depend strongly on frequency. In the following section we consider the effect on the RMS acceleration at a specific location on the cylinder wall to acoustic shot noise averaged over the fluid bed/wall interface.

### 4. Response of cylinder wall to acoustic shot noise

We introduce the transfer function,  $H(t-t',R_i)$ , that relates the time response of the wall acceleration, a(t,0), at R=0, to the force,  $F(t',R_i)$ , at time t' and location  $R_i$  through the usual convolution integral. For a force pulse generated by an impact hammer at location  $R_i$ , the transfer function is most simply expressed in frequency space by:  $a(f) \equiv a(f,0) =$  $H(f,R_i)F(f,R_i)$ , where a(f,0) is the Fourier transform of the acceleration at location R=0, and  $H(f,R_i)$  and  $F(f,R_i)$  the Fourier transform of the transfer function, and force at location  $R_i$ . From the Wiener-Khintchine theorem [34], we note that

$$S_{a}(f,0) = |H(f,R_{i})|^{2} S_{F}(f,R_{i})$$
(3)

From Eqs. (2) and (3), the acceleration power spectrum at location R = 0, due to random particle impact over the entire surface of the cylinder confining the fluid bed is given by

$$S_{a}(f,0) = \sum_{i=1}^{N} |H(f,R_{i})|^{2} [4m\rho_{m}v_{n}^{3}\Delta A_{i}]$$
 (3a)

We average over the surface area of the cylinder, A, and obtain,

$$S_{a}(f,0) = \langle |H(f)|^{2} \rangle \langle 4m\rho_{m}v_{n}^{3} \rangle A \tag{4}$$

where.

$$<|H(f)|^{2}> \equiv \frac{1}{A} \sum_{i=1}^{N} |H(f,R_{i})|^{2} \Delta A_{i}$$
  
=  $\frac{1}{N} \sum_{i=1}^{N} |H(f,R_{i})|^{2}$  (4a)

and

$$<4m\rho_{\rm m}v_{\rm n}^{3}> \equiv \left(\frac{1}{A<|H(f)|^{2}>}\right)\sum_{i=1}^{N}|H(f,R_{\rm i})|^{2}4m\rho_{\rm m}v_{\rm n}^{3}\Delta A_{\rm i}$$
(4b)

We have detected no significant change in  $S_a(f,0)$  with a change in the height of the fluid bed by factor of 50%, suggesting either that the weighting due to  $|H(f,R_i)|^2$  is not significant, or that  $4m\rho_m v_n^3$  varies little over the bed. In the following we shall consequently replace the weighted average  $<4m\rho_m v_n^3>$  by the bed average:  $4m\rho_m v_n^3$ , and write

$$S_a(f,0) = \langle |H(f)|^2 \rangle (4m\rho_m v_p^3 A) \tag{5}$$

Eq. (5) is the fundamental equation of this paper. It makes possible the quantitative coupling of the acoustic shot noise excitation of the wall of the vessel confining the fluid bed with the measurement of the average particle granular temperature within the bed.

The acceleration power spectrum in Eq. (5) can be measured at an arbitrary wall location adjacent to the bed. The averaged transfer function,  $<|H(f)|^2>$ , then depends upon the selected location. As will be seen,  $<|H(f)|^2>$ , can be estimated from a mechanical model of the response of the cylinder confining the bed. However, for quantitative measurement of the average granular temperature through Eq. (5), as well as a critical test of the mechanical theory underlying the measurement, we determine  $<|H(f)|^2>$  experimentally through impact hammer excitation.

## 5. Experimental determination of cylinder transfer function

The fluidized bed was contained within cylinders constructed of either Pyrex glass with an i.d. of 7.366 cm (2.9 in) and a wall thickness of 0.254 cm (0.10 in), or aluminum, with an i.d. of 7.62 cm (3.0 in) and a wall thickness of 0.635 cm (0.25 in). The materials and dimensions of the cylinders were chosen to test Eq. (5) against significant changes in  $\langle |H(f)|^2 \rangle$ . They also serve to minimize electrostatic effects due to charging of the glass spheres. For both cylinders, gas (dry helium or argon) was introduced into the fixed bed through a gas distributor made of a high density polyethylene porous membrane 1.9 cm (3/4 in) thick with  $40-60~\mu m$  pores. The pressure drop across the gas distributor was about a third of the pressure drop across the packed bed

The quantity  $\langle |H(f)|^2 \rangle$  was determined with the bed fluidized. A piezoelectric accelerometer (Bruel and Kjaer

4374) was attached to the cylinder with wax at a location 15.3 cm above the gas distributor and 3 cm below the bed height for the packed bed, and its charge output converted into a voltage by a charge amplifier (Bruel and Kjaer 2635). The spatially-averaged transfer function defined by Eq. (5),  $\langle |H(f)|^2 \rangle$ , was determined by hammer impact (Bruel and Kjaer 8203) at N locations such that  $N\Delta A_i = A$  (in our measurements, N = 100 - 200). At the center of each elemental area on the cylinder surface,  $\Delta A$ , at location  $R_i$ , 20 hammer impacts were averaged, and  $|H(f,R_i)|^2$  was obtained with a two channel signal processor (Bruel and Kjaer 2032). Subsequent average of  $|H(f,R_i)|^2$  over the surface area of the cylinder was then used to obtain  $\langle |H(f)|^2 \rangle$ .

## 6. Experimental validation of acoustic shot noise excitation of the cylinder wall

It is critical to note that the power spectra of non-coherent noise sources add and, consequently, the experimental value of  $S_{\rm a}(f,0)$  will, in general, have contributions other than the acoustic shot noise power spectrum given by Eq. (2). In order to utilize Eq. (5) to measure  $T^*$ , we have to find a frequency band in which acoustic shot noise is the dominant contribution to the response of the accelerometers.

We determined empirically the appropriate frequency range in two ways. The first is through the frequency dependence of the experimental quantity, R(f)

$$R(f) = \frac{S_{a}(f,0)}{\langle |H(f)|^{2} \rangle} \tag{6}$$

which should be independent of frequency if Eq. (5) is correct. Fig. 1 exhibits the measured acceleration power spectrum,  $S_a(f,0)$ , for the 3.0 in i.d. aluminum cylinder for glass spheres with  $D = 297 \mu m$ , fluidized with helium gas. We note

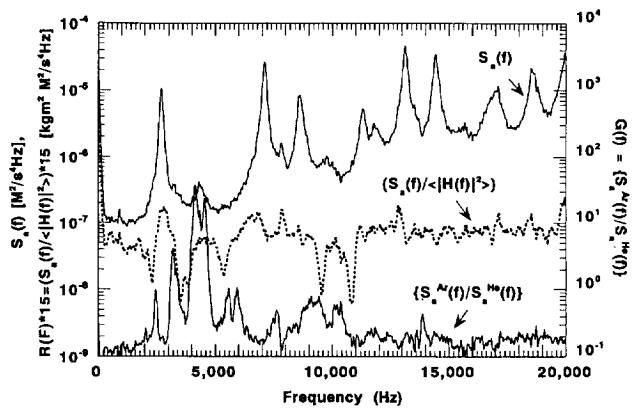


Fig. 1. The measured acceleration power spectrum,  $S_a(f,0)$  over the range 0–25.6 kHz for the 7.62 cm (3.0 in) i.d. aluminum cylinder containing glass spheres with  $D=297~\mu m$ , fluidized with helium gas. Also shown are the ratios, G(f), between  $S_a(f,0)$  and the measured average transfer function,  $<|H(f)|^2>$ , and R(f), of the acceleration power spectrum,  $S_a^{AC}(f,0)$ , taken with argon fluidization and the acceleration power spectrum  $S_a^{He}(f,0)$ , taken with helium fluidization. Both G(f) and R(f) are dominated by a white noise source in the frequency range 10–20 kHz.

that  $S_a(f,0)$  exhibits resonant peaks at frequencies corresponding to the resonances of the cylinder and the contained gas over the entire frequency range. In addition, we note that  $S_a(f,0)$  increases by a factor of 100 over the range 0–20 kHz.

In contrast, the ratio R(f) is constant within a factor of 2 over the same range and between 10 and 20 kHz is approximately independent of frequency. In this frequency band, the resonant peaks in  $S_a(f,0)$  simply reflect resonant peaks in  $< |H(f)|^2 >$ , and since their quotient,  $R(f) = [S_a(f,0)/< |H(f)|^2 >]$  is a weak function of frequency, we will assume  $R(f) = S_F(f) = (4m\rho_m v_n^3 A)$ 

The second approach to determining the appropriate frequency range is through changes in the fluidizing gas. Argon has a sound velocity of 319 m/s at 0 °C, compared with a sound velocity for helium of 965 m/s. The factor of three difference in sound velocity leads to a factor of three difference in the frequency of associated acoustic resonances for the two gasses. Supporting evidence that  $S_{\rm a}(f,0)$  is dominated by acoustic shot noise in the frequency band 10–20 kHz is obtained from the quantity G(f), where

$$G(f) = \frac{S_{\rm a}^{\rm Ar}(f,0)}{S_{\rm a}^{\rm He}(f,0)} \tag{7}$$

is the ratio of the measured acceleration power spectrum for two different fluidizing gasses, argon and helium. G(f) would be a constant if Eq. (5) were accurate. G(f) is thus a sensitive measure of the contribution of acoustic resonances to  $S_a(f,0)$ . Again from Fig. 1, we note that while G(f) exhibits resonances below 10 kHz, it is again weakly dependent on frequency in the band 10–20 kHz. It is interesting to note that in addition to their acoustic properties, argon and helium differ in viscosity (210 and 189 micropoise ( $\mu$ P), respectively, at 0 °C), a difference which accounts for the observed 10% shift in fluidization on-set derived from the RMS acceleration obtained for identical glass spheres fluidized by argon or helium gas.

From these two sets of experimental data we define 10-20 kHz, as the frequency band where acoustic shot noise is the dominant contribution to the acceleration power spectrum and where Eq. (4) can be used to determine the particle fluctuation velocity normal to the wall,  $v_{\rm n}$ . Similar experimental results and conclusions have been obtained for the glass cylinder.

In the fluidization experiments  $S_a(f,0)$  was obtained from the output of two accelerometers diametrically opposed and located at the same height above the gas distributor, utilizing the same charge amplifier and signal processor as in the impact hammer calibration, the only difference being the excitation source, impact hammer in one case, acoustic shot noise in the other. The experimental quantity of interest is the average RMS acceleration, a, which is the average of the square root of the integral of  $S_a(f,0)$ , taken over the frequency band 10–20 kHz for each accelerometer. There was no significant difference in the quantity, a, when the number of samples used to define  $S_a(f,0)$  was varied from 1000 (32 s

sampling time) or to 20 (0.6 s sampling time). In practice, 100 time samples were used (3.2 s sampling time). In no case did the RMS acceleration of the two accelerometers in the frequency range 10–20 kHz, differ by more than 10%.

With two accelerometers it is possible to probe for the degree of coherence or common signal between the two vibrational probes. The coherence ranges between 0 and 1. While coherences of the order of 0.6–0.5 were observed below 10 kHz corresponding to the acoustic and structural resonances shown in Fig. 1, above this frequency the average coherence is well below 0.1, again confirming random particle impact on the wall as the dominant contribution to the power spectrum.

The dominant visual feature of a fluidized bed is the upward movement of bubbles and the consequent convective flow of particles at the wall. In contrast, the particle motion that contributes to acoustic shot noise cannot be easily observed, but is the dominant feature of the high frequency portion of the wall power spectrum. The choice of 10–20 kHz as the measurement range for the RMS acceleration restricts the measured phenomena to those which occur in times faster than 0.1 ms, for example the impact time of particle at the wall. In contrast, the transit of bubbles past the accelerometers which occur in times of the order of 0.1-1 s corresponds to power spectral features below 10 Hz, in the same frequency range as that of the pressure fluctuations across a fluid bed [38]. It is important to note that while bubbles do not directly contribute to the RMS wall acceleration in the range 10–20 kHz they may contribute indirectly through their contribution to the average particle granular temperature.

Of course an additional critical test of the model is the independence of the derived particle normal velocity,  $v_n$ , on the construction of the cylinder and the material from which is made, which will be considered in the following section. A more subtle test of the model, to be discussed in a later section, is the fact that while large and significant changes in the wall construction of the cylinder have no change on the derived value for  $v_n$ , small percentage changes in particle diameter at and across the Geldart A/B boundary produce very significant changes in the dependence of the granular temperature on superficial gas velocity. All these experimental results strongly support the hypothesis that the acceleration power spectrum in the frequency range 10–20 kHz is dominated by acoustic shot noise due to random particle impact on the wall and as such can be quantitatively described by Eq. (5).

### 7. Summary of acoustic shot noise formulae

For the convenience of the reader, we now summarize the equations which we have utilized to convert a vibrational signal at the wall of the fluid bed to quantitative information on the particle granular temperature. The mean squared (MS) value of the acceleration,  $a^2$ , over the frequency range  $f_1 < f < f_2$ , is given by:

$$a^2 = MS$$
 acceleration:  $f_1, f_2 = \int_{f_1}^{f_2} s_a(f,0) df$  (8a)

For all the experimental data to be presented we take  $f_1 = 10$  kHz and  $f_2 = 20$  kHz, as discussed earlier. However, as noted that there are other sources of noise, both mechanical and electrical, which will be reflected in a noise contribution to the above integral. We designate that contribution as,  $S_n(f)$ , and the noise contribution to the MS acceleration,  $a_n$ . In general the experimental MS acceleration,  $a_m$  is given by

$$a_{\rm m}^2 \equiv \int_{f_1}^{f_2} [S_{\rm a}(f,0) + S_{\rm n}(f)] \, \mathrm{d}f = a^2 + a_{\rm n}^2$$
 (8b)

where  $a_n^2$  is determined by the electronic and, possibly, vibrational noise that is independent of acoustic shot noise and independent of gas flow. In our experiments electronic noise was dominant. In what follows we define  $a^2 = (a_m^2 - a_n^2)$ .

We define the quantity  $I^2$  in the same frequency range by

$$I^{2} = \int_{0}^{f_{2}} \langle |H(f)|^{2} \rangle df \tag{9}$$

and then from Eqs. (5) and (8)

$$v_{\rm n} = \left(\frac{a^2}{4I^2 A m \rho_{\rm m}}\right)^{1/3} = \left(\frac{1}{D\rho_{\rm o}^{1/3}\rho_{\rm m}^{1/3}}\right) \left(\frac{3}{2\pi I^2 A}\right)^{1/3} (a^{2/3}) \tag{10}$$

where, in the second expression, we consider spherical particles of diameter D, mass density  $\rho_{\rm o}$ , and solids fraction  $(1-\epsilon_{\rm s})$  such that  $\rho_{\rm m}=\rho_{\rm o}$   $(1-\epsilon_{\rm s})$ . Eq. (10) is the fundamental acoustic shot noise formula of this paper relating the measured values of a, I, A, m,  $\rho_{\rm m}$ , D, and  $\rho_{\rm o}$  to the RMS particle velocity  $v_{\rm n}$ . The granular temperature is then given by  $T^*=v_{\rm n}^2$ .

Table 1 gives the geometry of the glass and aluminum cylinders as well as the magnitude of  $I^2$  obtained from Eq. (9). We note that the quantity  $I^2A$  for the aluminum cylinder is 10 times less than that for the glass cylinder. As expected, the experimental data for  $v_n$  derived from the measured RMS acceleration, a, through Eq. (10) is independent of this difference.

The factor of 10 difference between the experimental magnitude of  $I^2A$  for the aluminum and glass cylinders can be ascribed to the factor of 2.5 difference in their wall thickness.

Table I
Geometry and average transfer function for aluminum and glass vessels

	Aluminum	Glass
Inner diameter (cm)	7.62 (3.0")	7.366 (2.9")
Wall thickness (cm)	0.635 (0.25")	0.254 (0.1")
Height (cm)	28	28
Outer area (cm <sup>2</sup> )	782	693
$I^2$ : 10–20 kHz (kg <sup>-2</sup> s <sup>-1</sup> )	$3.02 \times 10^{7}$	$3.22 \times 10^{8}$
$I^2A (m^2 kg^{-2} s^{-1})$	$2.36 \times 10^{6}$	$2.23 \times 10^{7}$

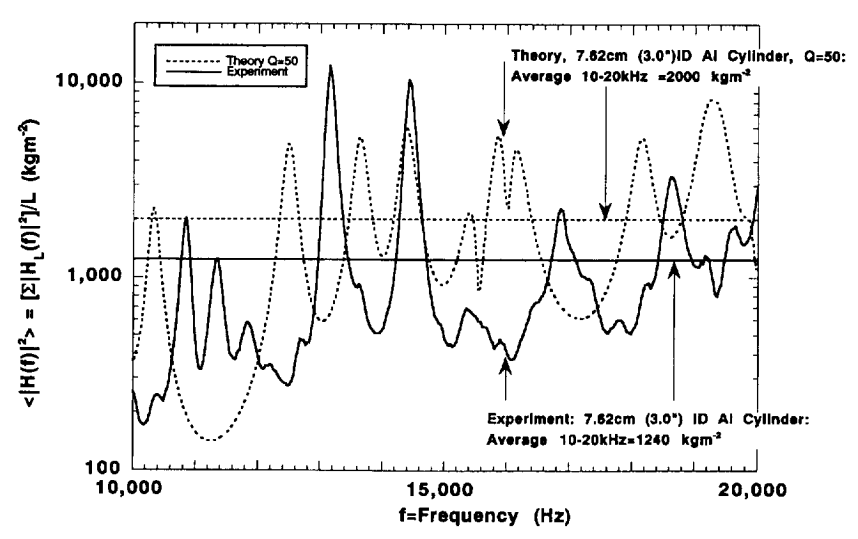


Fig. 2. Plot of experimental average transfer function,  $<|H(f)|^2>$ , for the 7.62 cm (3.0 in) i.d. aluminum cylinder for glass spheres with  $D=297~\mu m$  fluidized with helium gas as a function of frequency over the range 10-20~kHz. Also shown are the results of a theoretical calculation due to Norris for  $<|H(f)|^2>$ , where the only free parameter is the Q (quality factor or measure of resonance band width) of the cylinder resonances. The average of  $<|H(f)|^2>$  over the band 10-20~kHz is also indicated for experiment and theory.

Norris [39], has modeled the thin walled cylinder as a plate, and shown that

$$I^{2}A = K \left[ \frac{(f_{2}^{2} - f_{1}^{2})(1 - \sigma^{2})^{1/2}}{\alpha \rho^{2} h^{3} C_{c}} \right]$$
 (11)

where K is a numerical constant  $(K = \pi \sqrt{3}/4)$ ,  $\sigma$  is the Poisson ratio of the cylinder material,  $\rho$  is the density of the cylinder material,  $C_e$  is its extensional sound velocity, and his the wall thickness of the cylinder. Eq. (11) exhibits an inverse cubic dependence on h. The only free parameter in Eq. (11) is the quantity a, which is the cylinder damping. This quantity is related to the quality factor Q of the cylinder resonances by  $\alpha = 1/Q$ , or to the logarithmic decrement (LD) of the cylinder resonances by  $\alpha = LD/\pi$ . Excellent agreement is found between the measured value of  $I^2A$  in Table 1 and Eq. (11) with characteristic values of  $\alpha \approx 30-70$ . The inverse third power on wall thickness exhibited by Eq. (11) suggests that a local measurement of acoustic shot noise can be obtained by local thinning of the wall. In the rough walls found in field environments localization of the transfer function may serve the same purpose [40,41].

Norris [39] has also constructed a dynamic model of a thin-walled cylinder using thin shell theory. This model exhibits structural resonances and yields reasonable quantitative agreement with measurements of  $I^2A$  in the frequency range of interest. Fig. 2 compares his calculated mean squared transfer function  $<|H(f)|^2>$  defined by Eq. (4) with the experimental data for the same quantity where the only free parameter is the Q (quality factor or measure of resonance band width) of the cylinder resonances. There is a satisfactory agreement in magnitude as well as a qualitative agreement in structure between the calculated and measured value of  $<|H(f)|^2>$ .

### 8. Experimental determination of granular temperature

All the experimental data are based on the RMS acceleration, a defined by Eq. (8), as a function of gas flow through the bed. The gas flow is characterized by the gas superficial velocity,  $U_s$ , defined as the quotient of the gas flow through the bed in volume units per second to the cross-sectional area of the cylinder confining the fluidized bed. The physical gas velocity within the fluid bed is, of course, a random variable with a magnitude that is considerably larger than  $U_s$ .

The particles initially utilized in the present experiments were glass spheres (1600 Series, Spacer Grade Microbeads, Cataphote Inc., Jackson, MI, 90% true [maximum variation of  $\pm 6\%$  from average diameter]) of average diameter 595, 420, 297, 210, 149, 105, 88, 74 and 63  $\mu$ m and density  $\rho_0 = 2.46$  gm/cc. As shown in Fig. 3, these spheres span region B, and extend into region A of the Geldart plot, a remarkably useful classification of the fluidization characteristics of powders [21–23]. As noted earlier, this semi-empirical classification summarizes the behavior of fluidized beds made up of particles with a given density and average diameter. Region B, has the descriptor bubbles readily since for these particles, the gas superficial velocity,  $U_s$ , at minimum fluidization conditions,  $U_s = U_{\rm mf}$ , is less than the gas superficial velocity at minimum bubbling conditions,  $U_s = U_{mb}$ . For Geldart B particles,  $U_{\rm mf} > U_{\rm mb}$ , and the bed bubbles at minimum fluidization velocity. Region A, has the descriptor aeratable, since for these particles,  $U_{\rm mf} < U_{\rm mb}$  and the fixed bed fluidizes before bubbling. From empirical observation Geldart [22] determined the quantity  $U_{\rm mb}$  in the A region, and equating this quantity to  $U_{\rm mf}$  (see Eq. (14)) one obtains for mono-dispersed spheres the A/B boundary as  $D(\mu m)^* \rho_0$  $(gm/cc) \approx 296$ . Thus for glass spheres with  $\rho_0 = 2.5$  gm/cc, the A/B boundary is at  $D(\mu m) \approx 120 \mu m$ . Somewhat arbi-

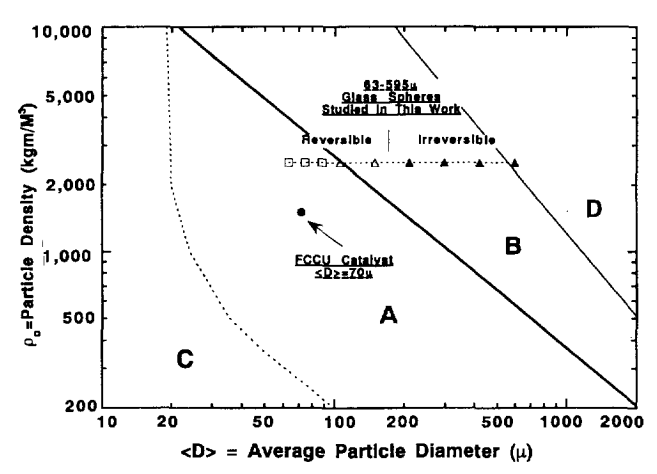


Fig. 3. Geldart's semi-empirical classification of the fluidization characterization of powders based on particle average density and particle average diameter is exhibited. Region A is designated **aeratable** since such powders fluidizes before bubbling. Region B is designated **bubbles readily** since such powders bubble at minimum fluidization conditions. The monodispersed glass spheres considered in this paper span region B and extend into region A. We also present data on a fluid bed catalytic cracking catalyst (PCCU) with a wide dispersion in shape and a log-normal distribution in particle diameter whose average density and diameter put it into region A.

trarily we place  $D(\mu \text{m}) \ge 105 \mu \text{m}$  in Geldart B, and less arbitrarily,  $D(\mu \text{m}) \le 88 \mu \text{m}$  in Geldart A.

Our measurements suggest that the Geldart classification is reflected in the dependence of the granular temperature on gas superficial velocity. As indicated in Fig. 3, we have discovered a remarkable change in the character of the fluidization transition as the A/B boundary is approached, from a hysteretic first order fluidization transition to a reversible second order fluidization transition. Reversible transitions continue to be found for the Geldart A particles as indicated by the open squares in Fig. 3.

An equally remarkable difference in the magnitude and functional dependence of the granular temperature on gas superficial velocity between Geldart A glass spheres and the Geldart B glass spheres has been discovered (see discussion following Figs. 7 and 8). This change may be understood as a reflection of enhanced coupling of the fluidization gas to the particles within the bed in the region  $U_{\rm mf} < U_{\rm s} < U_{\rm mb}$  due to the repression of bubbles.

The Geldart classification refers to average values of particle density and diameter. The glass spheres that are the focus of this paper differ significantly from fluidized catalytic cracking unit (FCCU) catalyst particles which, as shown in Fig. 3, also fall in region A. Such catalyst particles have a wide dispersion in both particle size and shape. This significant difference may be the source of the factor of 20–30 increase in bed collapse time [24,25] we observe (see Fig. 11) between such catalyst particles and the monodispersed glass spheres with the same average density examined in this paper.

In contrast, we have found no significant difference between the steady state behavior of the granular temperature for the Geldart A glass spheres and the Geldart A FCCU catalyst (compare Fig. 6 and Fig. 8). This result supports the concept that the difference between region A and region B, is not the bed collapse time, but rather fundamental differences in the role of gas/particle and particle/particle interactions within the fluidized bed [5].

The minimum fluidization velocity,  $U_{\rm mf}$ , can be estimated by equating the viscous pressure drop,  $\Delta P$ , across the fixed bed to the pressure drop given by the weight of the bed [1]. For fluid beds with a Reynolds number of the order of unity, the pressure drop,  $\Delta P$ , across the packed bed of height  $L_{\rm mf}$ , and solid fraction  $(1-\epsilon_{\rm mf})$  consisting of particles of diameter, D, due to flow of gas with viscosity,  $\mu_{\rm g}$ , at velocity  $U_{\rm mf}$ , obeys the semi-empirical expression

$$\frac{\Delta P}{L_{\rm mf}} = \frac{150(1 - \epsilon_{\rm mf})^2 \mu_{\rm g} U_{\rm mf}}{\epsilon_{\rm mf}^3 D^2}$$
 (12)

We equate the pressure drop given by the first term of Eq. (12) to the pressure drop due to the weight of solids of particle density  $\rho_0$  in the fluidized state,

$$\frac{\Delta P}{L_{\rm ref}} = (1 - \epsilon_{\rm mf}) \rho_{\rm o} g \tag{13}$$

where g is the gravitational constant (9.8 m/s<sup>2</sup>). Using empirical values for  $\epsilon_{\rm mf}$  ( $\epsilon_{\rm mf}$  = 0.3825),  $U_{\rm mf}$  is given by:

$$U_{\rm mf} = \frac{D^2 \rho_{\rm o} g}{1650 \mu_{\rm o}} \tag{14}$$

As will be considered later in this paper and shown in Fig. 11, the minimum fluidization velocity,  $U_{\rm mf}$ , predicted from Eq. (14) is within 10–20% of our experimental estimate of  $U_{\rm mf}$ , based on either the saturation of the pressure drop across the bed, the increase in bed height, or the vibrational measurement of  $T^*$  for glass spheres for which  $63 \le D \le 595 \ \mu {\rm m}$ .

Vibrational measurements of  $T^*$  have turned out to be a very convenient and sensitive probe of the fluidization transition. However, as shown in the following section, the use of  $T^*$  or the particle fluctuation velocity  $v_{\rm n}$ , defined by Eq. (10), to characterize the transition from a fixed to a fluidized bed, reveals a complexity that cannot be captured by the single parameter,  $U_{\rm mf}$ .

## 9. First order fluidization transition for Geldart B glass spheres: $210 \le D \le 595 \mu m$

For each diameter sphere we have studied the fluidization transition over two paths: Path 1, and Path 2. In what follows we assign the terms **up** and **down** to increasing and decreasing gas flow. For Path 1 transitions, the fluidization transition is started from conditions of zero gas flow,  $U_s = 0$  for at least 10 s, {1st up, 5th up}. For Path 2 transitions,  $U_s$  is never reduced to zero {2nd down, 3rd up, 4th down}. We have found that for spheres with diameters in the range,  $210 \le D \le 595~\mu m$  and Path 1 transitions, the fluidization transition always exhibits a discontinuous jump in  $v_n$ . In con-

trast, we have found for Path 2 transitions of spheres in this diameter range, the derived value of  $v_n$  is continuous and reversible.

Fig. 4 exhibits examples of this phenomena: Fig. 4(a) and (b) for glass spheres of diameter  $D=297~\mu m$  fluidized with helium in the glass cylinder, and in Fig. 4(c) and (d) for glass spheres of diameter  $D=210~\mu m$  fluidized with helium in the aluminum cylinder. For both cylinders we show the RMS acceleration, a, defined by Eq. (8) and the ratio of the particle fluctuation velocity,  $v_{\rm n}$ , defined by Eq. (10), to the gas superficial velocity,  $U_{\rm s}$ .

As noted, the discontinuous transition for Path 1 transitions, 1st up and 5th up, exhibited in Fig. 4, is a characteristic feature of the monodispersed glass spheres we have observed for  $210 \le D \le 595~\mu \mathrm{m}$ . The solid triangles in Fig. 3, correspond to these transitions. For these diameter spheres the fluidization transition for Path 1 conditions is always first order [42] with a discontinuous jump in both the RMS acceleration, a, or the derived sphere velocity,  $v_{\mathrm{n}}$ . In contrast, for Path 2 transitions where  $U_{\mathrm{s}} \ne 0$ , and either increasing or decreasing gas flow (2nd down, 3rd up, 4th down), the fluidization transition determined by a and  $v_{\mathrm{n}}$  is continuous and

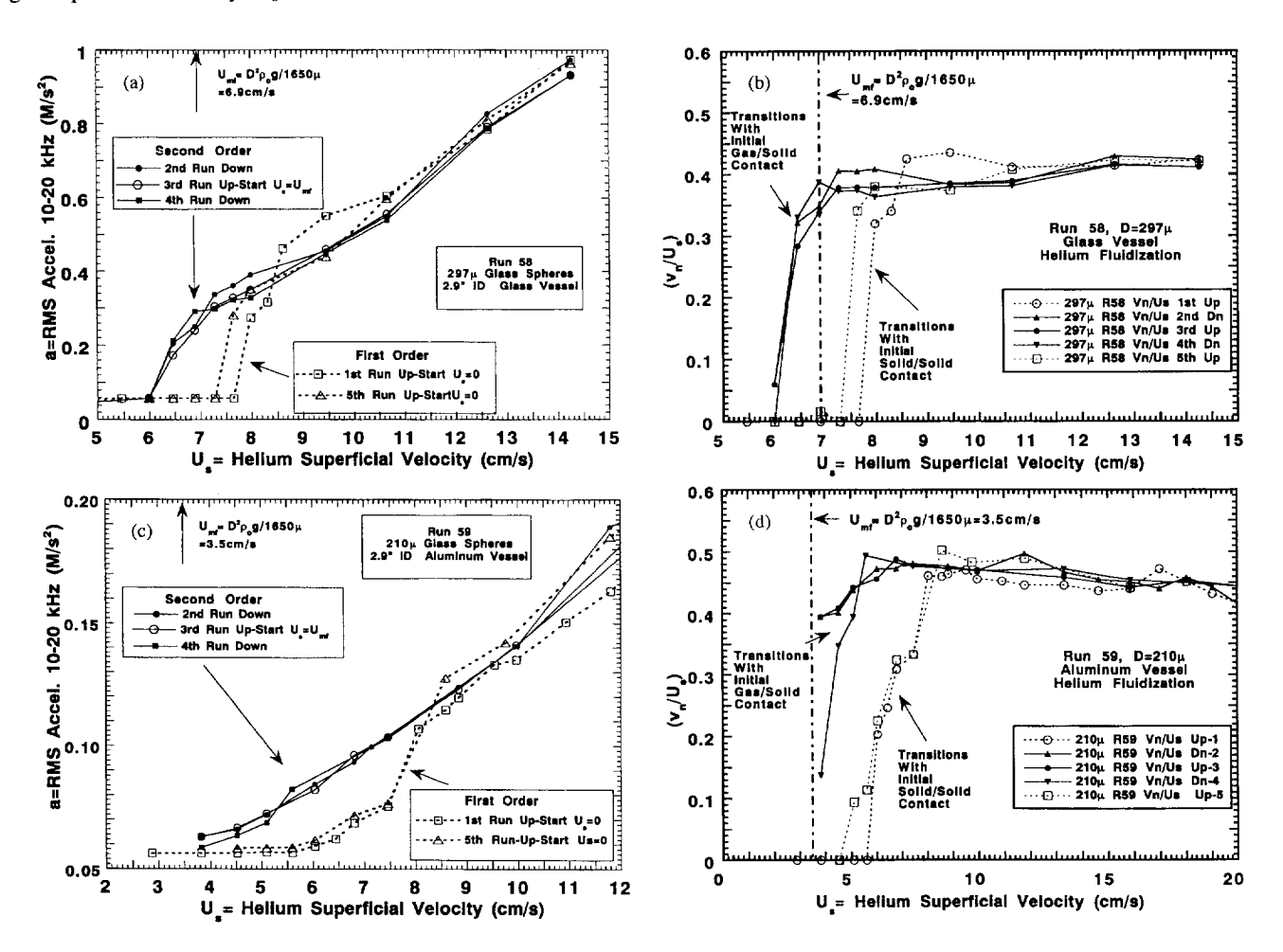


Fig. 4. (a) RMS acceleration as a function of gas superficial velocity for monodispersed glass spheres with  $D = 297 \mu m$  fluidized in the glass cylinder with 7.366 cm (2.9 in) i.d. with helium gas. As described in the text, the reversible transitions shown in Runs 2, 3 and 4 correspond to transitions where the gas superficial velocity is never set to zero. The hysteretic transitions shown in Runs 1 and 2 and Runs 4 and 5 correspond to transitions where the gas superficial velocity is set to zero for a few seconds, before Run 1, and after Run 4. (b) Ratio of sphere fluctuation velocity normal to the cylinder wall,  $v_n$ , derived from the data in Fig. 4(a), using Eq. (10), to the gas superficial velocity, as a function of gas superficial velocity for monodispersed glass spheres with  $D = 297 \ \mu \text{m}$ fluidized in the glass cylinder with 7.366 cm (2.9 in) i.d. with helium gas. As described in the text, the reversible transitions shown in Runs 2, 3 and 4 correspond to transitions where the gas superficial velocity is never set to zero. The hysteretic transitions shown in Runs 1 and 2 and Runs 4 and 5 correspond to transitions where the gas superficial velocity is set to zero for a few seconds, before Run 1, and after Run 4. (c) RMS acceleration as a function of gas superficial velocity for monodispersed glass spheres with  $D = 210 \mu m$  fluidized with helium gas in the aluminum cylinder with 7.62 cm (3.0 in) i.d. As described in the text, the reversible transitions shown in Runs 2, 3 and 4 correspond to transitions where the gas superficial velocity is never set to zero. The hysteretic transitions shown in Runs 1 and 2 and Runs 4 and 5 correspond to transitions where the gas superficial velocity is set to zero for a few seconds, before Run 1, and after Run 4. (d) Ratio of sphere fluctuation velocity normal to the cylinder wall,  $v_n$ , derived from the data of Fig. 4(a) using Eq. (10), to gas superficial velocity, as a function of gas superficial velocity for monodispersed glass spheres with  $D = 210 \mu m$  fluidized with helium gas in the aluminum cylinder with 7.62 cm (3.0 in) i.d. As described in the text, the reversible transitions shown in Runs 2, 3 and 4 correspond to transitions where the gas superficial velocity is never set to zero. The hysteretic transitions shown in Runs 1 and 2 and Runs 4 and 5 correspond to transitions where the gas superficial velocity is set to zero for a few seconds, before Run 1, and after Run 4.

reversible as shown in Fig. 4, and may be described as second order

Hysteresis in the fluidization transition has not been previously observed for particles in the Geldart B region, although it is a dominant feature of pressure and bed height monitors of the fluidization transition of Geldart A catalyst particles [43]. Our observation of path dependent transitions is independent of significant changes in the cylinder wall material and we do not believe that it is associated with surface charges or coatings. One explanation for this behavior is that Path 1 transitions for the monodispersed glass spheres are associated with sphere/sphere contact and van der Waals forces between the spheres. For Path 2 transitions, there is gas is always flowing and sphere/sphere contact is not present. However, as will be discussed the magnitude of the van der Waals energy [44] is such that it only plays a role for sphere diameters with diameters below  $\approx 10 \,\mu\text{m}$ , the Geldart C region of Fig. 2.

A more plausible explanation is that glass spheres for which  $210 \le D \le 595~\mu m$ , arrive at an untapped spatial configuration for the dense phase under the influence of gravity that is significantly different from the equilibrium dense phase of the fluidized state. To return to the language of thermodynamics, this model would ascribe the hysteresis of the Path 1 transitions to a significant difference in particle configurational entropy between the state of the dense phase at  $U_s \approx U_{\rm mf}$  and at  $U_s = 0$ .

## 10. Second order fluidization transition for Geldart B glass spheres: D=105 and 149 $\mu$ m

Strikingly different behavior has been found for the fluidization transitions of glass spheres with diameters D=105 and 149  $\mu$ m. As shown in Fig. 5, the fluidization transition as measured by RMS velocity  $v_{\rm n}$ , is always continuous and reversible irrespective of either: the fluidizing gas, the material of the confining cylinder, or the starting conditions of particle contact with respect to  $U_{\rm s}$ . For glass spheres with these diameters, the fluidization transition is thus always second order. As shown in Fig. 5, we can fit  $v_{\rm n}/U_{\rm s}$  by a function of  $U_{\rm s}$  that rises rapidly at  $U_{\rm s}/U_{\rm mf} \approx 1$ , and which saturates to a constant value at  $U_{\rm s}/U_{\rm mf} \geq 2$ .

As will be seen we have observed the same second order transitions for the Geldart A glass spheres we have examined as indicated in Fig. 3. Thus for glass spheres  $63 \le D \le 149~\mu m$ , the untapped configurational entropy of the dense phase is the same at  $U_{\rm mf}$  and at  $U_{\rm s}=0$ . We have found no reference in the literature to this remarkable dependence of the reversibility of the fluidization transition on the sphere diameter. Our use of aluminum and glass cylinders and glass spheres rules out the contribution of electrostatic effects either between the spheres or at the wall. It is significant that this change in the order of the transition occurs at the A/B boundary of the Geldart plot and continues into the Geldart A region.

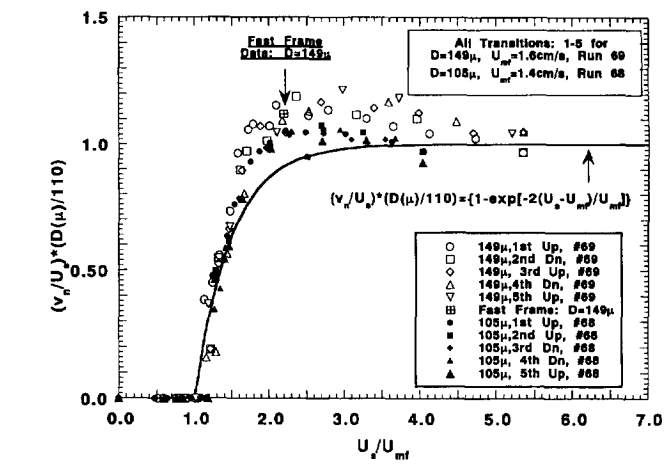


Fig. 5. Ratio of sphere fluctuation velocity normal to the cylinder wall,  $v_{\rm n}$ , to gas superficial velocity, multiplied by the ratio of sphere diameter in microns to the empirical constant  $D_{\rm o}=110~\mu{\rm m}$  for monodispersed glass spheres with D=149 and  $105\,\mu{\rm m}$  fluidized with argon gas in the glass cylinder with 7.366 cm (2.9 in) i.d. The data is displayed as a function of gas superficial velocity  $U_{\rm s}$  normalized to the minimum fluidization velocity,  $U_{\rm mf}$ . As described in the text, all the transitions are reversible independent of whether the gas superficial velocity is never set to zero (Runs 2, 3 and 4) or set to zero for a few seconds, before Run 1, and after Run 4. The empirical curve,  $\{1-\exp(-2[(U_{\rm s}/U_{\rm mf})-1)\}$  was chosen to fit the rapid rise in  $(v_{\rm n}/U_{\rm s})(D/110\,\mu{\rm m})$  for  $(U_{\rm s}/U_{\rm mf})\approx 1$ , its saturation for  $(U_{\rm s}/U_{\rm mf})\geq 1$ , and its independence of sphere diameter, D.

We have attempted to measure directly the fluctuation velocity by fast frame video and computer enhanced imaging to follow particle motion between collisions. For 149  $\mu$ m glass spheres fluidized in argon at  $U_{\rm s}=4$  cm/s we have obtained  $v_{\rm n}=3.3$  cm/s from this data. The agreement with  $v_{\rm n}$  obtained from the vibrational data shown in Fig. 5, is excellent. However the statistical scatter in the optical data is considerable ( $\pm50\%$ ), and unavoidable due to wall curvature and the low index of refraction of the glass spheres.

### 11. Granular temperature of Geldart B glass spheres

In Fig. 6 we exhibit the quantity  $((v_n/U_s) (D(\mu)/110))$  as a function of  $U_s/U_{mf}$  for 1st Up, Path 1 transitions for the suite of glass spheres displayed in the Geldart B region of Fig. 3. The experimental data for  $(v_n/U_s)$  scales with the sphere diameter, D, and is well approximated by an empirical function of  $(U_s/U_{mf})$  which rises and saturates rapidly as a function of  $(U_s/U_{mf})$ . For  $(U_s/U_{mf}) \ge 1$ :

$$\left(\frac{v_{\rm n}}{U_{\rm s}}\right) = \left(\frac{D_{\rm o}}{D}\right) \left[1 - \exp\left(\frac{-2(U_{\rm s} - U_{\rm mf})}{U_{\rm mf}}\right)\right] \tag{15}$$

Eq. (15) introduces a new parameter into the characterization of the fluidized state, the diameter scaling constant  $D_o$ . For the monodispersed glass spheres we have studied,  $D_o \approx 110 \, \mu \text{m}$ .

From Eq. (15), for  $U_{\rm s}/U_{\rm mf} \approx 1~(v_{\rm n}/U_{\rm s})$  is a linear function of  $(U_{\rm s}-U_{\rm mf})$ 

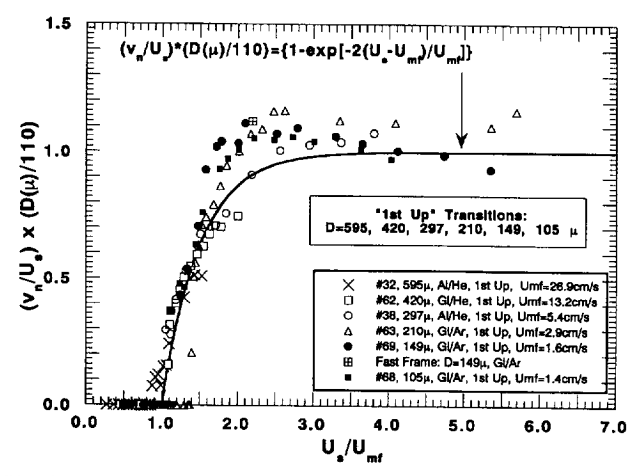


Fig. 6. Ratio of sphere fluctuation velocity normal to the cylinder wall,  $v_{\rm av}$  to gas superficial velocity, multiplied by the ratio of sphere diameter in  $\mu{\rm m}$  to the empirical constant  $D_{\rm o}=110~\mu{\rm m}$ . The data is displayed as a function of gas superficial velocity for monodispersed glass spheres falling into the Geldart B region of Fig. 3 with D=595, 420, 297, 210, 149, and 105  $\mu{\rm m}$ . As described in the text, all the transitions are Run 1, 1st Up. The empirical curve,  $\{1-\exp(-2\{(U_{\rm s}/U_{\rm mf})-1)\}\}$  was chosen to fit the rapid rise in  $(v_{\rm n}/U_{\rm s})(D/110\mu{\rm m})$  for  $(U_{\rm s}/U_{\rm mf})\approx 1$ , its saturation for  $(U_{\rm s}/U_{\rm mf})\geq 1$ , and its independence of sphere diameter, D.

$$\left(\frac{v_{\rm n}}{U_{\rm s}}\right) \approx \left(\frac{2(U_{\rm s} - U_{\rm mf})}{U_{\rm mf}}\right) \left(\frac{D_{\rm o}}{D}\right) \tag{16}$$

We have used Eq. (16) to determine experimentally  $U_{\rm mf}$  and find that it agrees with  $U_{\rm mf}$  determined from pressure drop across the bed, or the onset of bed expansion. As noted  $U_{\rm mf}$  determined by Eq. (16) agrees with that predicted by Eq. (14) within 20% for the Geldart B glass spheres.

For  $U_s/U_{\rm mf} \ge 2$ , the right-hand side of Eq. (15) is a constant and  $v_{\rm n}$  is a linear function of  $U_s$ , which is inversely proportional to the sphere diameter with a proportionality constant given by the quantity  $D_o$ 

$$v_{\rm n} = U_{\rm s} \left( \frac{D_{\rm o}}{D} \right) \tag{17}$$

Rathbone et al. [45] using fiber-optic doppler anemometry derived average particle normal velocities at the wall of  $v_{\rm n}\approx 0.15$  m/s for a fluidized bed consisting of 600–850  $\mu{\rm m}$  particles of sand at gas superficial velocities,  $U_{\rm s}\approx 0.7$  m/s. These measurements yield  $v_{\rm n}/U_{\rm s}\approx 0.2$  in reasonable agreement with the magnitude predicted by Eq. (17),  $v_{\rm n}/U_{\rm s}\approx 0.15$  for an estimated average particle diameter of  $< D>\approx 725~\mu{\rm m}$ .

For  $U_s \approx U_{\text{mf}}$ , the granular temperature of the dense phase spheres at the wall, from Eq. (17) is given by:

$$T^* = \langle v_{\rm n}^2 \rangle \approx \left[ \frac{2(U_{\rm s} - U_{\rm mf})}{U_{\rm mf}} \right]^2 \left[ \frac{D_{\rm o}^2}{D^2} \right] U_{\rm s}^2$$
 (18a)

and, for  $U_s/U_{ref} \ge 2$ :

$$T^* = \langle v_{\rm n}^2 \rangle \approx \left(\frac{D_{\rm o}^2}{D^2}\right) U_{\rm s}^2 = \left(\frac{D_{\rm o}^2}{D^2}\right) \left(\frac{U_{\rm s}}{U_{\rm mf}}\right)^2 U_{\rm mf}^2$$
 (18b)

and if we replace  $U_{\rm mf}$  by Eq. (14) we obtain at  $U_{\rm s}/U_{\rm mf}=2$ 

$$T^* = \langle v_{\rm n}^2 \rangle \approx 4 \left( \frac{D}{D_{\rm o}} \right)^2 \left( \frac{D_{\rm o}^2 \rho_{\rm o} g}{1650 \,\mu_{\rm o}} \right)^2$$
 (18c)

The quadratic dependence of the granular temperature on  $U_s$  in Eq. (18a) is expected on dimensional grounds, the inverse quadratic dependence of  $T^*$  on D and consequent introduction of the scaling constant  $D_o$  has not been reported in previous experiments or obtained theoretically. Koch [14] considered a dilute monodispersed gas of elastic particles translating through a viscous gas. If we make the implausible assumption that the particle drift velocity is much less than the gas velocity, we obtain from this model,  $T^* \approx (U_s^{4/3}/D^{2/3})$ , which is considerably different from Eq. (18b).

We can utilize Eq.(18) to determine the critical particle diameter  $D_{\rm vw}$  where the sphere kinetic energy, KE, is equal to the van der Waals interaction energy, Q. From Eq. (18c) we obtain at  $U_{\rm s}/U_{\rm mf}=2$ 

$$KE = \frac{3}{2} \left[ \frac{\pi}{6} \rho_{o} D^{3} \right] T^{*} = \left( \pi \rho_{o} D_{o}^{3} \right) \left( \frac{D^{5}}{D_{o}^{5}} \right) \left( \frac{D_{o}^{2} \rho_{o} g}{1650 \mu_{o}} \right)^{2}$$
(19)

Substituting  $\rho_o = 2.5$  gm/cc,  $\mu_g = 200 \mu P$ , and  $D_o = 110 \mu m$ , we obtain  $KE \approx 8 \times 10^{-6} \ (D/D_o)^5$  ergs. From Fuchs [44]  $Q \approx 2 - 5 \times 10^{-13}$  ergs for quartz, and hence  $KE \le Q$  for  $D \le 3-4 \ \mu m \approx D_{vw}$ . In Fig. 3 the transition between the Geldart A and Geldart C regime where cohesive forces dominate fluidization occurs at a sphere diameter of 20  $\mu m$ .

The results shown here for the granular temperature, may supply insights into the relative role of gravitational and inertial effects in the mechanics of the dense phase of a fluidized bed made up of Geldart B particles. For example we can define an inertial or granular pressure,  $P^* = \rho_m T^*$ , from Eq. (18). The ratio of the inertial pressure to the gravitational pressure across a layer whose thickness is one sphere diameter,  $\rho_m gD$ , is

$$Fr = \left(\frac{v_{\rm n}^2}{gD}\right) = \left(\frac{D_{\rm o}}{D}\right)^2 \left(\frac{U_{\rm s}}{U_{\rm mf}}\right)^2 \left(\frac{U_{\rm mf}}{gD}\right) \tag{20a}$$

The quantity Fr will be recognized as the Froude number, a non-dimensional hydrodynamic parameter that characterizes the relative importance of inertial forces compared to gravitational forces [46]. At  $U_{\rm s}/U_{\rm mf}\approx 2$ , replacing  $U_{\rm mf}$  by Eq. (14) gives,

$$Fr = \left(\frac{D_o \rho_o}{1650 \mu_g}\right)^2 (4gD) = 2.7 \times 10^{-3} D \ (\mu \text{m})$$
 (20b)

where we have substituted  $\mu_{\rm g}=200~\mu{\rm P},~D_{\rm o}=110\mu,$   $\rho_{\rm o}=2.5{\rm gm/cc},~g=9.8~{\rm m/s^2}.$  For the glass spheres that span Geldart's region B, at  $U_{\rm s}/U_{\rm mf}=2$ ,  $Fr=1.6\to0.3$  for  $D=600\to100~\mu{\rm m}$ , suggesting comparable magnitudes of inertial, gravitational, and of course, viscous forces, in the dense phase of this fluidization regime.

Eq. (20) would predict that inertial forces would play a decreasing role for particle diameters that are in the Geldart

A region. However, we note that for these particles the bed fluidizes before bubbling, and one might anticipate a higher granular pressure due to enhanced gas flow in the dense phase. As will be seen in the next section, the experimental data support this conjecture.

# 12. Granular temperature of Geldart A particles: monodispersed glass spheres and FCCU catalyst particles

As indicated in Fig. 3, we have made measurements on monodispersed glass spheres with diameters D=88,74, and 63  $\mu$ m respectively, which extend the granular temperature measurements into the A region of the Geldart diagram. In this Geldart region the minimum fluidization velocity is less than the minimum velocity for bubbling. Such spheres should exhibit significantly different fluidization properties than Geldart B powders and presumably significantly granular temperature. It is gratifying that the experimental data support this conjecture. The data reveal a dramatic change in the dependence of the granular temperature on gas superficial velocity with the 20% change in particle diameter required to cross the A/B boundary in the Geldart diagram (105  $\rightarrow$  88  $\mu$ m).

In Fig. 7 we show the results of four experimental runs on glass spheres with  $D=63~\mu\mathrm{m}$ . The data are reversible, similar to the measurements that had been made on glass spheres on the B side of the A/B boundary of Fig. 3. However, as noted, we find a remarkable change in both the functional dependence of  $(v_n/U_s)(D/D_o)$  on  $U_s/U_{\mathrm{mf}}$ , and its magnitude in the range  $1 \le U_s/U_{\mathrm{mf}} \le 2$ .

Fig. 8 compares the fluctuation velocity for spheres with D=63, 74, and 88  $\mu$ m and we note similar scaling with the particle diameter, D, as was observed for the Geldart B glass

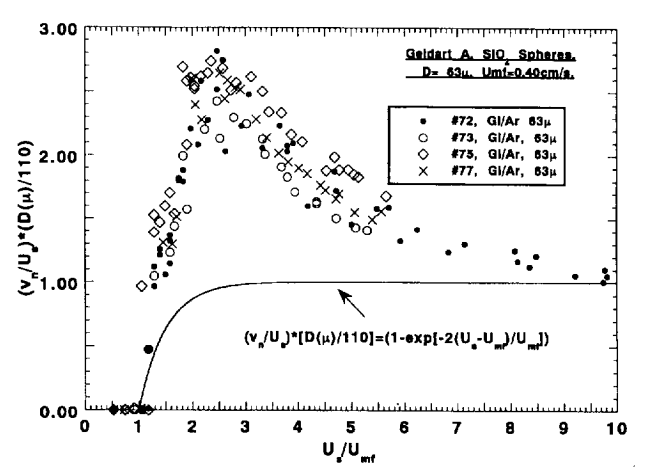


Fig. 7. Ratio of sphere fluctuation velocity normal to the cylinder wall,  $v_{\rm n}$ , to gas superficial velocity, multiplied by the ratio of sphere diameter in  $\mu{\rm m}$  to the empirical constant  $D_{\rm o}=110~\mu{\rm m}$  for four experimental runs for Geldart A monodispersed glass spheres with  $D=63~\mu{\rm m}$ . All the transitions are reversible, independent of whether the gas superficial velocity is not set to zero (Runs 2, 3 and 4) or set to zero for a few seconds, before Run 1, and after Run 4. The exhibited curve is the empirical one shown in Fig. 6.

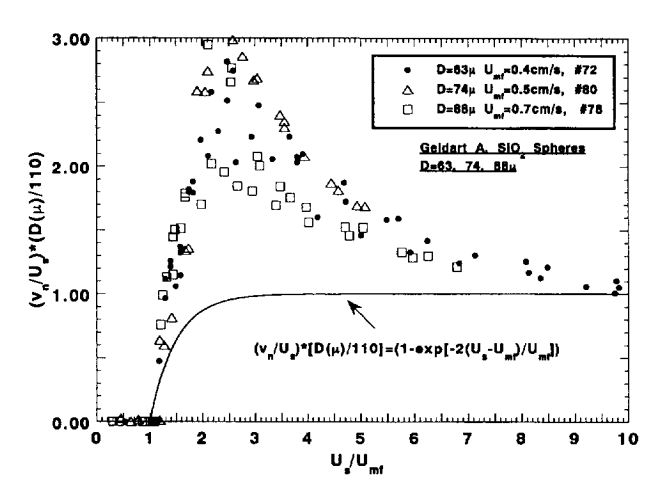


Fig. 8. Ratio of sphere fluctuation velocity normal to the cylinder wall,  $v_{\rm in}$  to gas superficial velocity, multiplied by the ratio of sphere diameter in  $\mu {\rm m}$  to the empirical constant  $D_{\rm o}=110~\mu {\rm m}$  for four experimental runs for Geldart A monodispersed glass spheres with D=88,74, and 63  $\mu {\rm m}$ . All the transitions are reversible, independent of whether the gas superficial velocity is not set to zero (Runs 2, 3 and 4) or set to zero for a few seconds, before Run 1, and after Run 4. The exhibited curve is the empirical one shown in Fig. 6.

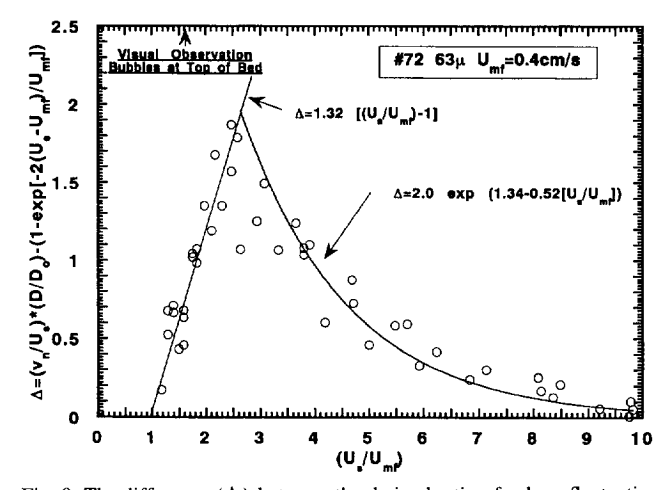


Fig. 9. The difference ( $\Delta$ ) between the derived ratio of sphere fluctuation velocity normal to the cylinder wall,  $v_{\rm n}$ , to gas superficial velocity, multiplied by the ratio of sphere diameter in  $\mu{\rm m}$  to the empirical constant  $D_{\rm o}=110~\mu{\rm m}$  for Geldart A monodispersed glass spheres with  $D=63\mu$  and the empirical curve used to fit the data for the Geldart B glass spheres shown in Fig. 6. The quantity  $\Delta$  can be approximated by a straight line up to  $U_{\rm s}/U_{\rm mf}\approx 2.6$  and an exponential for  $U_{\rm s}/U_{\rm mf} \gtrsim 2.6$ .

spheres. The data shown in Fig. 8 suggests a similar universal functional dependence on  $(U_{\rm s}/U_{\rm mf})$  for Geldart A glass spheres, but one that is dramatically different from that observed for Geldart B glass spheres.

In Fig. 9 we show the difference,  $\Delta(U_s/U_{mf})$ , between the solid curve given by Eq. (15) and the experimental data for  $D=63~\mu m$  (Run 72). We see that  $\Delta$  is reasonably approximated by a function of  $(U_s/U_{mf})$  that exhibits a linear rise for  $1 \le (U_s/U_{mf}) \le 2.5$  to a maximum which is followed by an exponential fall-off to  $(v_n/U_s)(D/D_o) \approx 1$  with a decay constant of the order of 2. As noted in Fig. 9, the simplest interpretation of the form of  $\Delta(U_s/U_{mf})$  is that it arises from

the suppression of bubbling up to  $U_{\rm s}/U_{\rm mf} \approx 2.5$  (we note bubbles at top of bed at  $U_{\rm s}/U_{\rm mf} \approx 1.6$ ), and an exponential shift to a bubbling regime comparable to Geldart B spheres at  $(U_{\rm s}/U_{\rm mf}) \approx 10$ .

At the point of the maximum for  $\Delta (U_{\rm s}/U_{\rm mf})$ ,  $(v_{\rm n}/U_{\rm s})$  ( $D/D_{\rm o}$ )  $\approx 2.5$  implying an increase in the granular temperature by a factor of 9 over the Geldart B spheres. Thus, for the Geldart A glass spheres, near  $U_{\rm s}/U_{\rm mf}\approx 2$ , the Froude number Fr (Eq. (20) is given by  $Fr\approx 2\times 10^{-2}{\rm D}(\mu{\rm m})$ . For Geldart A glass spheres with  $D=88\to63~\mu{\rm m}$ , we note that  $Fr\approx 2\to 1$ , implying a greatly enhanced role for inertial forces for Geldart A glass spheres compared to that extrapolated from the Geldart B regime.

We have also obtained granular temperature data for another class of Geldart A particles, FCCU catalysts. We have examined two such catalyst particles, Quasar 4452 and Aczo Advance 817, with similar physical properties: density, 1.5 gm/cc and a log-normal distribution in particle diameter with a median diameter of 70  $\mu$ m and  $\sigma$  of 35  $\mu$ m. Scanning electron micrographs (SEM) show that both catalysts are non-spherical with very rough surfaces. Fig. 10 exhibits  $(v_{\rm p}/U_{\rm s})(D/D_{\rm o})$  for these catalysts, and we note qualitative and semi-quantitative similarity with the data shown in Fig. 8 for the Geldart A glass spheres. Again all the transitions are reversible. There is a similar peak in  $(v_p/U_s)(D/D_o)$  and a similar exponential fall off at high values of  $U_s/U_{\rm mf}$  for both the catalyst particles and glass spheres, suggesting that this behavior is a general feature of Geldart A particles which is independent of particle roughness or dispersion.

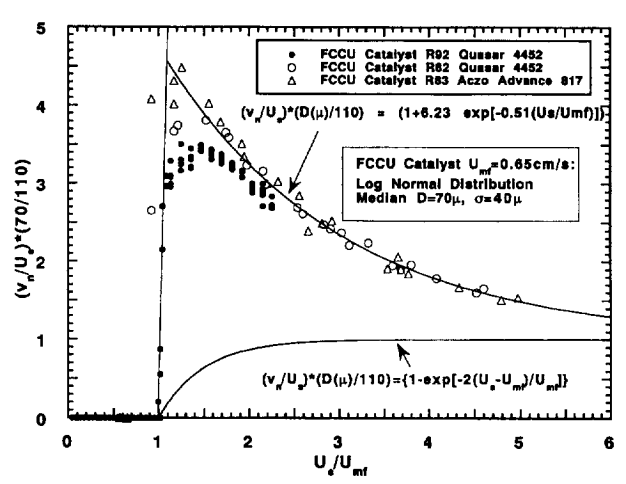


Fig. 10. Ratio of sphere fluctuation velocity normal to the cylinder wall,  $v_{\rm n}$ , to gas superficial velocity, multiplied by the ratio of sphere diameter in  $\mu {\rm m}$  to the empirical constant  $D_{\rm o}=110~\mu {\rm m}$  for two catalytic cracking catalysts. These catalysts, Quasar 4452 and Aczo Advance 817 have similar physical properties and their mean diameter and density places them in the Geldart A classification of Fig. 3. All the transitions are reversible independent of whether the gas superficial velocity is not set to zero (Runs 2, 3 and 4) or set to zero for a few seconds, before Run 1, and after Run 4. The experimental data is compared to the empirical curve used to fit the data for the Geldart B glass spheres shown in Fig. 6. The fitted curve is exponential with similar constants as that utilized in Fig. 9. The transition to the exponential occurs for  $U_{\rm s}/U_{\rm mf}\approx 1.5$ .

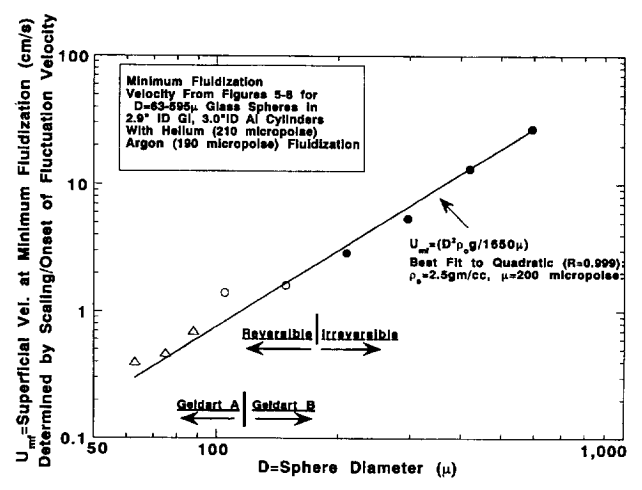


Fig. 11. Minimum fluidization velocity for the Geldart A and B glass spheres ( $\rho_0 = 2.5 \text{ gm/cc}$ ) derived from the onset of fluidization determined by the RMS acceleration and exhibited in Figs. 5–10. The straight line is Eq. (14) for  $\mu_e = 200 \mu \text{P}$  and  $\rho_0 = 2.5 \text{ gm/cc}$ .

It is noteworthy that the decay constant of the exponential for the catalyst particles is the same, within experimental error, as that observed for the glass spheres. In contrast, the magnitude of the peak in  $(v_n/U_s)(D/D_o)$  for the catalyst particles is approximately 30% larger than that observed for the glass spheres, possibly reflecting either the lower density of the particles, or the effect of the wide dispersion in particle sizes. The Froude number near  $U_{\rm mf}$  from Eq. (20) is again of the order of 1. However, we note from Fig. 10, that the transition to the exponential occurs near  $U_s/U_{\rm mf} \approx 1.2-1.5$ , about a factor of two less than that observed for the Geldart A spheres.

No significant difference was observed between  $U_{\rm mf}$  determined by pressure drop, bed height, or  $(v_{\rm n}/U_{\rm s})$  for either the Geldart A or B glass spheres. For the catalyst particles,  $U_{\rm mf}=0.65$  cm/s, was derived from the  $(v_{\rm n}/U_{\rm s})$  measurements. This value of  $U_{\rm mf}$  is about a factor of three larger than the minimum fluidization velocity defined by either the bed pressure drop or the bed height. This significant difference may be due to the broad dispersion in particle diameter, surface, and/or shape found in the FCCU catalyst particles.

Fig. 11 summarizes the measurement of  $U_{\rm mf}$  for the glass spheres as a function of particle diameter. There is general agreement with Eq. (14) based on a mean viscosity of 200  $\mu$ P and  $\rho_{\rm o}=2.5$  gm/cc. Two transitions are observed for the glass spheres. For sphere diameters between D=210 and  $D=149~\mu{\rm m}$ , the fluidization transition becomes reversible and remains so. For sphere diameters between D=105 and  $D=88~\mu{\rm m}$  the dependence of  $(v_{\rm n}/U_{\rm s})(D/D_{\rm o})$  on  $U_{\rm s}/U_{\rm mf}$  changes dramatically as shown in Fig. 8. Both transitions appear to be correlated with the Geldart A/B boundary.

In the experimental literature, the most significant difference between Geldart A and Geldart B particles has been the difference in the time scales of bed collapse [22,24]. In the following section we shall discuss our measurements of bed collapse for Geldart B and A glass spheres, and Geldart A

1.05

catalyst particles. We shall also present the first measurements of the time dependence of the granular temperature during bed collapse for Geldart B spheres.

## 13. Bed collapse measurements: Geldart A and B, monodispersed glass spheres and Geldart A, FCCU catalyst particles

Collapse tests have been widely used to characterize the properties of the dense phase of a fluid bed. In such tests, the supply of gas to the bed is abruptly cut off and bed height and other fluidization parameters are monitored as a function of time. In his review, Grace [24] presents measurements of bed height as a function of time for a fluid catalytic cracking catalyst with a median diameter of about 60 µm fluidized at 1.9 cm/s. These catalyst particles have a normal dispersion in particle diameter ( $\sigma = 18 \mu m$ ) and unspecified roughness and shape. Based on mean particle diameter, they fall into region A of the Geldart classification (Fig. 3). The bed height for such catalyst particles is an approximate linear function of time and decays to its value at minimum fluidization in about 18 s for collapse under double over-vented conditions. It is generally accepted in the literature that such long collapse times are characteristic of Geldart A powders; in contrast, Geldart B particles collapse very rapidly when the gas supply is cut off [22].

We have examined both bed height and granular temperature as a function of time for the Geldart A and B glass spheres, and Geldart A fluid catalytic cracking catalyst in our own apparatus. Bed height was determined by fast frame video imaging using a NAC HSV-400 Color High Speed Video at 200 color images a second illuminated by a 250 ms strobe. The catalytic cracking particles (Quasar 4452) had a log-normal distribution with a mean diameter of 70  $\mu$ m ( $\sigma$  = 35  $\mu$ m).

The bed collapse measurements are shown in Fig. 12(a) and, on an expanded scale, in Fig. 12(b). As anticipated, the collapse curve for the catalyst particles exhibited a similar time dependence to that observed by Grace [24]. The time scale for the collapse,  $\approx 12$  s, is comparable to Grace's data and to that observed in pressure drop measurements by Chen and Weinstein [25]. As indicated in Fig. 12(a) and (b), the collapse curves for monodispersed Geldart A glass spheres with  $D=74~\mu m$  exhibited collapse times  $T_{\rm col}\approx 0.6$  s which are more than an order of magnitude shorter than for the catalyst particles, and only a factor of two greater than that observed for the Geldart B glass spheres with  $D=105~\mu m$  ( $T_{\rm col}\approx 0.3$  s).

Bed expansion is another parameter used to probe the difference between the Geldart A and B regions. As indicated in the expanded scale of Fig. 12(b), Geldart A glass spheres exhibit slightly more expansion for the same value of  $(U_s/U_{\rm mf})$  (1.09 compared to 1.07). In contrast, FCCU catalyst particles exhibit considerably more expansion than the Geldart A glass spheres (1.20 compared to 1.09). If we define

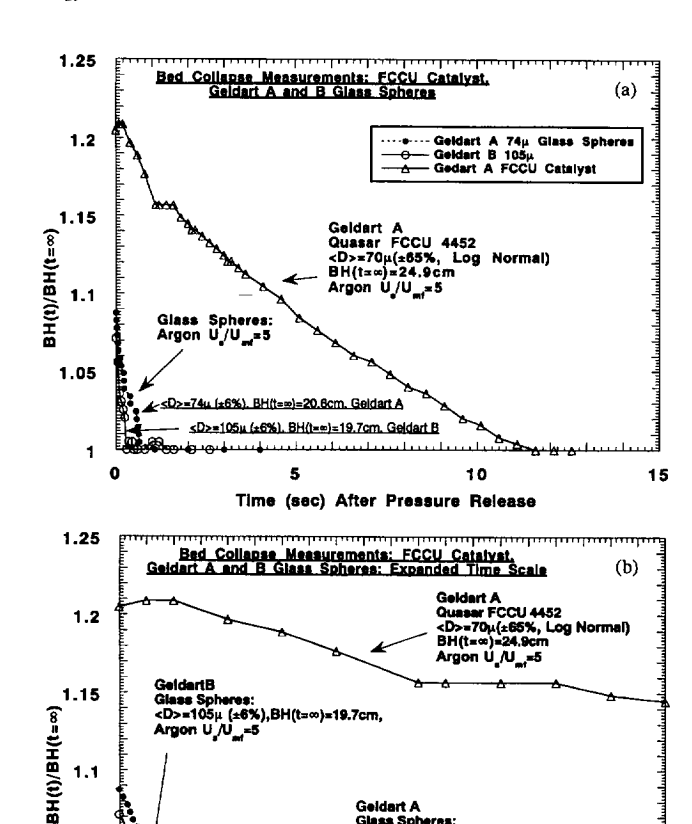


Fig. 12. (a) Time dependence of bed height, BH(t), after doubly vented bed collapse for Geldart A and B monodispersed glass spheres. The data was obtained by a strobe illuminated fast frame video as described in the text. (b) Expanded scales for the time dependence of bed height, BH(t), after doubly vented bed collapse for Geldart A and B monodispersed glass spheres and Geldart A FCCU catalyst particles. The data was obtained by a strobe illuminated fast frame video as described in the text.

1

Time (sec) After Pressure Release

1.5

0.5

the collapse velocity,  $V_{\rm col}$  as the change in bed height with collapse from  $U_{\rm s}/U_{\rm mf}$ ,  $\Delta BH$ , divided by the collapse time,  $T_{\rm col}$ , we obtain for the Geldart A glass spheres with D=74  $\mu$ m,  $V_{\rm col}\approx 3$  cm/s, and for the spheres with D=105  $\mu$ m at the A/B boundary,  $V_{\rm col}\approx 5$  cm/s, about an order of magnitude more rapid than the collapse velocity for the catalyst particles.

The fundamental distinction between Geldart A and B glass spheres is clearly not the decay time of bed collapse, but rather the remarkable change in the dependence of the granular temperature on gas superficial velocity exhibited in Figs. 7–9. This view is consistent with the concept that the dynamics of Geldart A particles are fundamentally different from Geldart B particles and this difference plays a key role in the suppression of bubbling [5,47]. Finally, Fig. 12 suggests that the long time scales observed for catalyst particles in bed collapse may be a granular effect on particle motion arising from the wide dispersion in particle size, shape, and roughness, and one which may not be an intrinsic feature of Geldart A particles.

## 14. Time dependence of granular temperature during bed collapse

The time dependence of the granular temperature of the glass spheres during bed collapse has also been measured. Before we consider these results in detail we consider the several time scales associated with bed collapse. One time scale is the time it takes for the bed height to fall to its fixed bed value during bed collapse,  $T_{col}$ , which, for the monodispersed glass spheres that lie adjacent to the Geldart A/B boundary, ranges from 0.3 to 0.7 s (Fig. 12(b)). Another time scale is the dependence of the average pressure drop across a fixed bed consisting of glass spheres of the same height as the experimental fluid bed. For glass spheres of diameter D, fluidized with helium, at close packing  $(\epsilon_s = 0.385)$ , in a bed of height  $L_s$ , a simple one-dimensional calculation leads to an exponential time dependence with a time constant  $T_g = (L_s^2/\pi^2 D_g)$ , where  $D_g = 1.3 \times 10^3$  $(D(\mu m)/100)^2$  cm<sup>2</sup>/s, is the gas diffusion coefficient for the packed spheres. For  $L_s = 18$  cm, and  $D = 150 \mu \text{m}$ ,  $T_g \approx 11$ 

The time dependence of the granular temperature for the Geldart B glass spheres during bed collapse under double vent conditions [24] is shown in Fig. 13 for 295  $\mu$ m glass spheres fluidized in helium in the glass cylinder at  $U_s/U_{\rm mf}\approx 5$ . The relative time sequence in Fig. 13 is characteristic of all the data we have obtained for the time dependence of the RMS acceleration, a(t), and the pressure drop at the gas distributor, p(t). In these measurements, the RMS acceleration, a(t), has been obtained by band pass filtering over the band 10–20 kHz, and converted to RMS values of acceleration at time t. Activation of the solenoid valves is indicated by the electrical transient at 650 ms. The pressure drop across the bed p(t) starts to fall about 100 ms after solenoid activation and initially falls to 1/e of its initial value

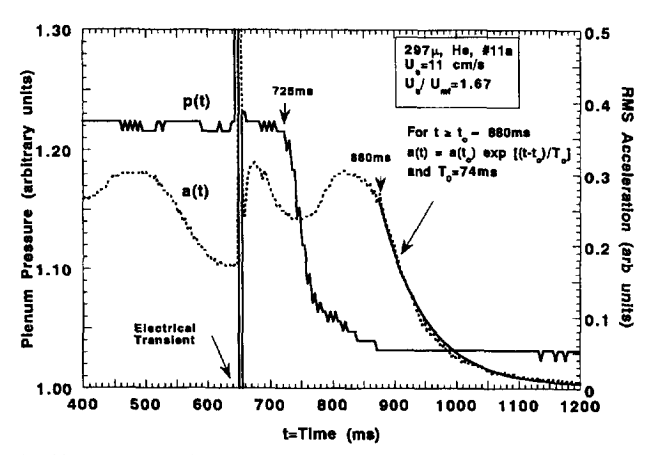


Fig. 13. Time dependence of plenum pressure drop, p(t), and RMS acceleration, a(t) taken over the band 10-20 kHz as described in the text, during bed collapse for monodispersed glass spheres with  $D=297~\mu m$  fluidized with helium gas at  $U_s=11~cm/s$ . The electrical transient at pressure release is indicated. The fitted curve to a(t) is an exponential with a time constant of 74 ms.

in approximately 7 ms, and approximately 90 ms later the plenum pressure drop, p(t), falls to zero.

The maximum in a(t) in the time interval between the first change in p(t) and its fall to atmospheric pressure seen in Fig. 13 is found for all the data. The peak in a(t) is produced by an initial increase in  $T^*$  in the dense phase that may result from the rapid collapse of the bubbles and the transfer of gas to the dense phase. The time dependence of a(t) after the peak has been found to be exponential. In the example shown in Fig. 13,  $a(t) \approx a(0) \exp(-t/T_0)$  with a time constant,  $T_0 \approx 74$  ms. A weak dependence of  $T_0$  on  $T_0$  is observed, which can be fit by a constant and a quadratic term with large scatter. For glass spheres with  $T_0 \approx 149$ , 210 and 295  $T_0 \approx 149$ , in helium and argon gas, for  $T_0 \approx 149$ , we obtained an exponential time constant,  $T_0 \approx 60-100$  ms.

The quantity  $T_{\rm o}$  is thus significantly larger than  $T_{\rm g}$  ( $\approx 11$  ms), the time it takes for the average pressure within the bed to fall to zero, and considerably less than  $T_{\rm col}$  ( $\approx 300$  ms), the time for bed collapse shown in Fig. 12(b). We will assume that  $T_{\rm o}$  is a measure of the time dependence of the sphere kinetic energy and explore the consequences of that assumption by considering a simple model for the time dependence of the granular temperature.

### 15. Langevin equation of particle motion

The observed experimental steady state of constant  $T^*$  for the dense phase of the fluid bed, requires power to supply the loss of energy due to inelastic particle/particle collisions. To estimate this power we utilize a Langevin equation [48–50] for the vector velocity c of the sphere,

$$m\frac{\mathrm{d}\boldsymbol{c}}{\mathrm{d}t} + m\frac{\boldsymbol{c}}{\tau_p} = \boldsymbol{F}(\boldsymbol{r},t) \tag{21}$$

where F(r,t) is a vector random force on the particle arising from gas/sphere interactions, and  $\tau_p$  is the relaxation time of the sphere velocity. We take the scalar product of both sides of Eq. (21) with c and time/ensemble average to obtain an expression for the steady state granular temperature,  $T^*$ :

$$T^* + \frac{V^2}{3} = \frac{\langle c \cdot c \rangle}{3} = \left(\frac{\tau_p}{3m}\right) \langle F \cdot c \rangle \tag{22}$$

where  $V = \langle c \rangle$ . In the following discussion we shall continue to neglect  $(V^2/3)$  with respect to  $T^*$  as discussed earlier. The quantity  $\langle F \cdot c \rangle$  is the work done on one sphere per unit time. The power input into the bed, dE/dt, is thus given by,

$$dE/dt = AL_s \rho_b < F \cdot c > \tag{23a}$$

where A is the cross-sectional area of the bed,  $L_{\rm s}$  is the bed height at the gas superficial velocity  $U_{\rm s}$ . An alternative expression for the power input into the bed required to maintain a steady state granular temperature in the dense phase is given by an equivalent pressure drop across the fluid bed,  $\Delta P_{\rm ke}$ ,

$$dE/dt = (AU_s)(\Delta P_{ke}) \tag{23b}$$

We equate Eq. (23a) and (23b) and, with Eqs. (18b) and (22), obtain for  $U_s/U_{mf} \ge 2$ ,

$$\Delta P_{ke} = \frac{3\rho_{m}L_{s} < v_{n}^{2} >}{\tau_{p}U_{s}} = \left(\frac{L_{s}(1 - \epsilon_{s})3\rho_{o}}{D^{2}}\right)\left(\frac{D_{o}^{2}}{\tau_{p}}\right)U_{s}$$
(24)

To estimate the magnitude of  $\Delta P_{\rm ke}$ , we take the ratio of Eq. (24) to the viscous pressure drop,  $\Delta P_{\rm visc}$ , across a fixed bed with the same voidage utilizing Eq. (12). We obtain for the ratio of  $\Delta P_{\rm ke}$  to  $\Delta P_{\rm visc}$  for  $U_{\rm s}/U_{\rm mf} \ge 2$ 

$$\frac{\Delta P_{\text{ke}}}{\Delta P_{\text{visc}}} = \left(\frac{1}{K}\right) \left(\frac{D_{\text{o}}^2}{\tau_{\text{o}}}\right) \left(\frac{\rho_{\text{o}}}{\mu_{\text{o}}}\right) \tag{25}$$

The numerical factor,  $K=50(1-\epsilon_{\rm s})/\epsilon_{\rm s}^3$ , contains the dependence on bed voidage. For the range of voidage found in fluidized beds, K changes by a factor of 2, from K=550, at  $U_{\rm s}/U_{\rm mf}\approx 1$ , to  $K\approx 260$ , at  $U_{\rm s}/U_{\rm mf}=2$ . We define  $(D_{\rm o}^2/\tau_{\rm p})$  as a kinetic energy diffusion constant, and we note from Eq. (25) that the ratio of the two pressure drops is a measure of the ratio of inertial  $(D_{\rm o}^2/\tau_{\rm p})$  and viscous  $(\mu_{\rm g}/\rho_{\rm m})$  diffusion constants.

From Eq. (25), for  $U_{\rm s}/U_{\rm mf} \approx 2$ ,  $D_{\rm o} \approx 110~\mu{\rm m}$ ,  $\mu_{\rm g} \approx 200~\mu{\rm P}$  and  $\rho_{\rm o} \approx 2.5~{\rm gm/cc}$ , for Geldart B glass spheres

$$\Delta P_{\rm ke}/\Delta P_{\rm visc} \approx 6/\tau_{\rm p} \, \rm ms$$
 (26a)

As shown in Fig. 8, Geldart A glass spheres exhibit a factor of 2.5 increase in  $(v_n/U_s)(D_o/D)$  for  $U_s/U_{mf} \approx 2$  and hence for these spheres.

$$\Delta P_{\rm ke}/\Delta P_{\rm visc} \approx 30/\tau_{\rm p} \,\,{\rm ms}$$
 (26b)

We next estimate the quantity  $\tau_p$ .

From the Langevin equation (Eq. (21)), the time dependence of the granular temperature  $T^*$ , when the power input into the bed (gas flow) is turned off, is given by

$$T^*(t) = T^*(0)\exp(-2t/\tau_{\rm p}) \tag{27}$$

Since from Eq. (10)  $a(t) \propto [T^*(t)]^{3/4}$ 

$$a(t) = a(0)\exp(-t/T_0) = a(0)\exp(-3t/2\tau_p)$$
 (28)

From Eq. (28), and the experimental value,  $T_{\rm o} = 60{\text -}100$  ms, we obtain an estimate of the Langevin kinetic energy relaxation time,  $\tau_{\rm p} = (3T_{\rm o}/2) \approx 90{\text -}150$  ms.

The magnitude of  $\tau_p$  can also be estimated from a consideration of the inelastic collisions between spheres. The loss of energy of the sphere in one collision defines a coefficient of restitution,  $e_p$  which measures the kinetic energy loss in one collision. We define  $T_I$  as the time for one collision, and equate the energy loss in that collision to the loss predicted by the Langevin equation in a collision time:

$$\frac{1}{2}(1 - e_{\rm p}^2) = \frac{2T_{\rm I}}{\tau_{\rm p}} \tag{29}$$

The time for one collision,  $T_1$  is of the order of  $D/v_n$ . For Geldart B spheres at  $U_s/U_{\rm mf} = 2$ ,  $T_1$  can be approximated by

$$T_{\rm I} \approx \frac{D}{v_{\rm p}} = \frac{1650\mu_{\rm g}}{2D_{\rm o}\rho_{\rm o}g} \tag{30}$$

Substituting  $D_0 = 110 \ \mu\text{m}$ ,  $\mu_g = 200 \ \mu\text{P}$ , and  $\rho_o = 2.5 \ \text{gm/cm}^3$ , we obtain from Eq. (30)  $T_1 \approx 6 \ \text{ms}$ .

We substitute  $T_1 = 6$  ms, and  $\tau_p = 90-150$  ms, into Eq. (29) and obtain  $e_p = 0.86-0.92$ , in excellent agreement with theoretical and experimental estimates of the coefficient of restitution for hard sphere collisions for materials with comparable hardness [51,52].

It is interesting to note that the above argument can be reversed to independently deduce the sphere fluctuation velocity. We substitute  $e_p = 0.9$ , and  $\tau_p = 90-150$  ms in Eq. (29) and estimate  $T_1 = 5-8$  ms. For D = 210  $\mu$ m, and the assumption that  $v_n = D/T_1$  we estimate  $v_n = 2-4$  cm/s, in satisfactory agreement with the value derived from acoustic shot noise through Eq.(18),  $v_n \approx 3$  cm/s.

We return to Eq. (26a,b). For  $\tau_{\rm p} \approx 90$ –150 ms, we obtain from Eq. (26a), for the Geldart B glass spheres at  $U_{\rm s}/U_{\rm mf} \approx 2$ ,  $(\Delta P_{\rm ke}/\Delta P_{\rm visc}) \approx 4$ –7%, and for the Geldart A glass spheres,  $(\Delta P_{\rm ke}/\Delta P_{\rm visc}) \approx 20$ –40%. Clearly the inertial contribution to particle dynamics cannot be neglected for particles in either Geldart classification, but there is a remarkable enhancement of the Froude number in the Geldart A regime.

The factor or factors that determine the scaling constant  $D_o$  remain a significant challenge for theory. The analysis shown here suggests that the significant theoretical quantity is not  $D_o$ , but rather  $D_o^2/\tau_p$ . For Geldart B spheres in the dense phase and  $U_s/U_{\rm mf} \approx 2$ , from the Langevin equation, and our experimental result for  $T^*$ , the time average power per unit volume due to sphere/sphere and sphere gas interactions,  $\mathscr P$  is given by

$$\mathscr{P} = \left(\frac{3\rho_{\rm m}U_{\rm s}^2}{D^2}\right)\left(\frac{D_{\rm o}^2}{\tau_{\rm n}}\right) \tag{31}$$

From Eq. (31) the steady state generation and dissipation of kinetic energy in the dense phase is also proportional the constant  $(D_0^2/\tau_p)$ .

We may also use the Langevin equation to obtain the relation between the power spectrum for the random velocity, c(t) and the power spectrum for the random force, F(r,t). We assume that this power spectrum is independent of frequency and given by  $S_F(f) = \mathcal{G}$ . It can be easily shown from the same argument that leads to the fluctuation-dissipation theorem [48], that the quantity  $\mathcal{G}$  is given by

$$\mathcal{G} = \left(\frac{2m^2T^*}{\tau_{\rm p}}\right) = \left(\frac{2m^2U_{\rm s}^2}{D^2}\right)\left(\frac{D_{\rm o}^2}{\tau_{\rm p}}\right)$$
(32)

Again the ratio  $D_o^2/\tau_p$ , rather than  $D_o$  alone appears to be the fundamental parameter.

### 16. Kinetic theory of dense gas of granular temperature $T^*$

We use these new results for  $T^*$  to calculate the inertial pressure, sound velocity, viscosity and diffusion constant of

the dense phase of a gas fluidized bed through a somewhat simplistic extension of the kinetic theory of dense hard sphere gasses [53]; a more rigorous treatment is given by Gidaspow [15]. We believe that the derived functional dependence of these quantities on gas superficial velocity, particle diameter and density, is accurate, although the magnitudes of the derived quantities are only known within a factor of order of unity. We continue to assume that the fluctuation velocity is isotropic at the wall, a necessary assumption, but one whose limitations can only be obtained by further experiment.

## 17. Kinetic theory of dense gas of granular temperature $T^*$ : inertial pressure $P^*$

The inertial pressure of the dense phase,  $P^*$ , is readily derived from kinetic theory as  $P^* = \rho_{\rm m} T^*$  and from Eq. (18b) for  $U_{\rm s}/U_{\rm mf} \ge 2$ ,

$$P^* = \rho_{\rm m} T^* = \rho_{\rm m} U_{\rm s}^2 \left( \frac{D_{\rm o}^2}{D^2} \right) = \rho_{\rm m} U_{\rm ml}^2 \left( \frac{D_{\rm o}^2}{D^2} \right) \left( \frac{U_{\rm s}^2}{U_{\rm ml}^2} \right)$$
(33)

We note for constant  $\rho_{\rm m}$ ,  $P^*$  is inversely proportional to  $D^2$  and directly proportional to  $U_{\rm s}^2$ . Based on the data presented in Fig. 11, we utilize Eq. (14) to obtain at a fixed value of  $(U_{\rm s}/U_{\rm mf})$ 

$$P^* \approx (\rho_{\rm m} D^2) \left( \frac{D_{\rm o} \rho_{\rm o} g}{1650 \mu_{\rm g}} \right)^2 \left( \frac{U_{\rm s}}{U_{\rm mf}} \right)^2$$
 (34)

For 500  $\mu$ m glass spheres fluidized in a gas with viscosity,  $\mu_g = 200 \ \mu$ P, at  $(U_s/U_{mf}) = 1$ ,  $P^* = 20 \ dynes/cm^2$ . At constant  $(U_s/U_{mf})$ ,  $P^*$  is directly proportional to  $D^2$ .

Campbell and collaborators [37,54,55] present data on the particle normal stress on the wall of a fluidized bed by a capacitive technique in which a perforated 12 mm diameter membrane is inserted in the wall of the fluid bed with gas pressure and particle normal stress on its front surface and only gas pressure on its back surface. The displacement is directly proportional to the difference in pressures on the two sides and hence proportional to the particle normal stress. The measurements of Campbell and collaborators are local and may be susceptible to local flow conditions, unlike the present measurements which average over the entire dense bed. Their elegant concept of separating the small particle pressure from the orders of magnitude larger gas pressure, by permitting gas flow, but not particle flow, behind the membrane may also have dynamic limitations.

We assume that the normal stress is of the same order as the granular pressure  $P^*$  and also assume an isotropic fluctuation velocity so that  $T^* = v_{\rm n}^2$ . Table 2 exhibits the average value and standard deviation of the quantity  $(v_{\rm n}/U_{\rm s})$   $(D(\mu)/110)$  for glass spheres of 500 and 1200  $\mu$ m diameter obtained from the paper of Campbell and Wang [54]. From Eq. (17), we would predict  $(v_{\rm n}/U_{\rm s})(D(\mu)/110) \approx 1$ , and the last column shows that the data derived from the normal stress measurements is in agreement with this prediction within a factor of 2.

Polashenski and Chen [56] have also made normal stress measurements by a technique similar to that of Campbell and collaborators and express their results in terms of the granular temperature at the wall. Table 3 is derived from Fig. 13 of their paper, and exhibits the average value and standard deviation of the quantity  $(v_n/U_s)$   $(D(\mu)/110)$  for sand particles

Table 2 Fluctuation velocity normal to wall,  $v_n$ , estimated from wall normal stress measurements of Campbell and collaborators [37,54,55]

Particle diameter, D	P*	$U_{ m s}$	$v_{ m n}$	$(v_{\rm n}/U_{\rm s})$	$(v_{\rm p}/U_{\rm s})(D(\mu{\rm m})/110)$
(µm)	(mm water)	(cm/s)	(cm/s)		·
1200	1.2	80	9.36	0.12	1.28
1200	18.6	150	38.65	0.26	2.81
1200	18.6	250	40.53	0.16	1.77
500	3	25	14.55	0.58	2.65
500	7.3	40	22.7	0.57	2.58
500	20	60	39.4	0.66	2.98
500	21	120	38.49	0.32	1.46
Average				0.38	2.22
Standard deviation				0.22	0.70

Table 3
Scaling of particle normal velocity derived from wall granular temperature of Polashenski and Chen [56]

Material	< D(μm) >	Range $U_s$ (m/s)	$<(v_n/U_s)(D(\mu m)/110)>$ in range of $U_s$	Standard deviation of $<(v_n/U_s)(D(\mu m)/110)>$ in range of $U_s$
Sand	283	0.2–0.8	1.1	0.3
Sand	1063	0.5-0.9	1.7	0.4
FCCU catalyst	94	0.1-0.4	0.6	0.1

with  $\langle D \rangle = 283$  and 1063  $\mu$ m, and FCCU catalyst particles with  $\langle D \rangle = 94$   $\mu$ m. Again we find agreement with Eq. (17) within a factor of 2.

The inertial stress/granular pressure measurements of the granular temperature are based on the zero frequency average of Eq. (1). The granular temperature measurements of the present paper are derived from a measurement of the acoustic shot noise power spectrum (Eq. (2)) over the frequency band 10–20 kHz. It is a remarkable validation of the acoustic shot noise probe as a measure of the wall granular temperature, that such different measurements are in such reasonable agreement.

Finally we note from Eq. (34), that  $P^*$  increases rapidly with increasing gas flow to the fluidized bed. At face value, this implies a necessary expansion of the dense phase and hence increasing gas flow through the dense phase. This conclusion is at variance with some two phase models for the fluidized state where it is assumed that, with increasing gas flow, the dense phase of the fluid bed remains at minimum fluidization conditions and that excess gas flows through the bubbles [57,58]. If Eq. (34) is an accurate description of the particle inertial pressure in the dense phase, models for gas flow through a bubbling fluidized bed may require revision.

## 18. Kinetic theory of dense gas of granular temperature $T^*$ : inertial sound velocity, $C^*$

The inertial sound velocity,  $C^*$  is given by  $C^{*2} = \mathrm{d}P^*/\mathrm{d}\rho_\mathrm{m} = T^*$ . From Eq. (18b) for  $U_\mathrm{s}/U_\mathrm{mf} \ge 2$ , we obtain

$$C^* = (D_o/D) U_s = \left(\frac{D_o U_{\rm mf}}{D}\right) \left(\frac{U_s}{U_{\rm mf}}\right)$$
(35)

Based on the data presented in Fig. 11, we again utilize Eq. (14) to obtain

$$C^* \approx D \left( \frac{D_o \rho_o g}{1650 \mu_o} \right) \left( \frac{U_s}{U_{cs}} \right) \tag{36}$$

At constant  $(U_s/U_{mf})$ ,  $C^*$  is linear in D.  $C^*$  is of the order of 3-4 cm/s for 74-100  $\mu$ m glass spheres at  $U_s/U_{mf} \approx 5$ .

There are a variety of sound waves that have been predicted and in some cases observed in fluidized beds [59–62]. Of course, the sound velocity that is measured in a specific experiment depends critically on the coupling between source and medium, and detector and medium. It is interesting to note that the bed collapse velocity,  $V_{\rm col} \approx \Delta BH/T_{\rm col}$ , which we have observed for Geldart A and B monodispersed glass spheres is in excellent agreement with the magnitude of  $C^*$  defined by Eq. (36).

## 19. Kinetic theory of dense gas of granular temperature $T^*$ : inertial viscosity, $\mu^*$

The inertial viscosity of a dense hard sphere gas,  $\mu^*$ , is given by  $\mu^* = (\sqrt{3}m/2\sqrt{2}\pi D^2)(T^*)^{0.5}$ , where we have

assumed a collision cross-section given by  $\pi D^2$ . From Eq. (18b) for  $U_s/U_{\rm mf} \ge 2$  we obtain

$$\mu^* = (\sqrt{3\rho_0 D_0} / 12\sqrt{2}) U_s \tag{37}$$

We note that the inertial viscosity is proportional to the superficial velocity and independent of diameter. Based on the data presented in Fig. 11, we again utilize Eq. (14) to obtain

$$\mu^* = \left(\frac{\sqrt{3}D_{o}\rho_{o}U_{mf}}{12\sqrt{2}}\right)\left(\frac{U_{s}}{U_{mf}}\right) \approx D^2 \left(\frac{D_{o}\rho_{o}^2g}{16167\mu_{g}}\right)\left(\frac{U_{s}}{U_{mf}}\right)$$
(38)

At  $U_{\rm s}/U_{\rm mf}\approx 2$  for a fluid bed consisting of glass spheres with  $D\approx 290~\mu{\rm m}$ , fluidized with helium ( $\mu_{\rm He}=190~\mu{\rm P}$ ), ( $\mu^*/\mu_{\rm He}$ )  $\approx 200$ . At constant ( $U_{\rm s}/U_{\rm mf}$ ), the ratio, ( $\mu^*/\mu_{\rm He}$ ), increases as  $D^2$ .

Gidaspow, Tsuo and Luo [63] calculate values of  $\mu^*$  for circulating and bubbling fluidized beds of 500  $\mu$ m glass spheres and obtain magnitudes of the order of 3–10 P for gas superficial velocities of the order of 5 m/s. For glass spheres at  $U_s = 5$  m/s we find  $\mu^* \approx 1.4$  P from Eq. (37).

There is only limited experimental data on the viscosity of fluidized beds. Early experimental data obtained from paddle wheel measurements in fluidized beds by Furukawa and Ohmae [64] quote similar magnitudes of  $\mu^*$ , but at considerably lower values of  $U_s$ . Rotating cylinder measurements of Schugerl [65] gave viscosities of the order of 10 P at  $U_s \approx 1-10$  cm/s for smooth glass spheres with the data again approximately independent of sphere diameter ( $D \approx 50-200$   $\mu$ m). However,  $\mu^*$  from Eq. (37) is two to three orders of magnitude smaller at these values of  $U_s$ . Recent experimental data on the viscosity of a catalytic cracking catalyst referenced by Gidaspow and Huilin [66] gives a value of  $\mu^* \approx 0.2$  P at  $U_s = 300$  cm/s. From Eq. (37)  $\mu^* = 0.3$  P for  $\rho_o = 1$  gm/cc and  $U_s = 300$  cm/s.

## 20. Kinetic theory of dense gas of granular temperature $T^*$ : inertial diffusion constant, $D^*$

The inertial diffusion constant of a hard sphere gas,  $D^*$ , is given by  $D^* = (D/2)(T^*)^{0.5}$ , where we have assumed a mean free path given by D/2. From Eq. (18b) for  $U_s/U_{\rm mf} \ge 2$ ,  $D^* = (D_o/2)U_s$  and is independent of sphere diameter D. For  $U_s = 0.1$  cm/s,  $D^* = 7 \times 10^{-4}$  cm<sup>2</sup>/s. Zik and Stavans [67,68] utilized a vibrated rather than fluidized bed, and found at a sphere convective velocity of 0.1 cm/s, a diffusion constant of  $3 \times 10^{-4}$  cm<sup>2</sup>/s, in reasonable agreement with the value predicted by Eq. (18) from the dense gas kinetic model.

For completeness we again utilize the data presented in Fig. 11, to obtain from Eq. (14)

$$D^* = (D_o/2) U_s \approx D^2 \left( \frac{D_o \rho_o g}{3300 \mu_e} \right) \left( \frac{U_s}{U_{mf}} \right)$$
 (39)

At constant  $(U_s/U_{mf})$ ,  $D^*$  has a quadratic dependence on D. From Eq. (39) for 300  $\mu$ m glass spheres fluidized with helium at  $(U_s/U_{mf}) = 2$ ,  $D^* \approx 7 \times 10^{-2}$  cm<sup>2</sup>/s.

### 21. Conclusions

The usefulness of the granular temperature concept has been questioned, particularly since "there appears to be no direct evidence that thermalized particle motion occurs in fluidized beds" [69]. This paper presents new experimental data on the granular temperature  $T^*$  and demonstrates its usefulness in characterizing a wide variety of fluid bed phenomena for monodispersed glass spheres that span the Geldart A and B regions.

We have introduced a novel experimental probe of the average granular temperature,  $T^*$ , in the dense phase at the wall of a fluidized bed, acoustic shot noise. We have validated this experimental probe in a variety of ways:

- (i) directly, through the robustness of the measured value of  $T^*$  with respect to significant changes in the elastic and acoustic properties of the materials of the cylinder confining the bed, and the acoustic and viscous properties of the fluidization gas;
- (ii) indirectly, through the internal consistency of the data for monodispersed glass spheres falling within either Geldart region A or B;
- (iii) indirectly, through the remarkable change that occurs in the magnitude of  $T^*$  near minimum fluidization as the Geldart A/B boundary is crossed for glass spheres with D=105 and 88  $\mu$ m;
- (iv) directly, through comparison with values for the granular temperature derived from particle normal stress on the wall.

We have demonstrated the versatility of the probe through the first measurements of the time dependence of  $T^*$  in bed collapse measurements.

We have demonstrated the utility of the granular temperature concept characterizing fluidization phenomena in several ways:

- (i) the discovery of the universal dependence of  $T^*$  on sphere diameter and gas superficial velocity for glass spheres that lie in the Geldart B region;
- (ii) the discovery of a dramatic change in the fluidization transition for Geldart B spheres as the Geldart A/B boundary is approached;
- (iii) the discovery of an equally dramatic change in the dependence of the granular temperature on gas superficial velocity as the Geldart A/B boundary is crossed and measurements made within the A region.

This data supports the concept that the distinction between Geldart A and B fluidization regimes lies in a fundamental difference in gas particle dynamics rather than an ad-hoc inhibition of bubbling.

The scaling of the experimental data we have obtained for the granular temperature has introduced a new characteristic length,  $D_{\rm o}$ , which for the glass spheres,  $D_{\rm o} \approx 110~\mu{\rm m}$ . When  $D_{\rm o}$  is combined with a Langevin velocity relaxation time,  $\tau_{\rm p}$ , a kinetic energy diffusion constant is introduced,  $D_{\rm o}^2/\tau_{\rm p}$ , which determines the power required to maintain the fluid bed in a steady state. The dependence of both these parame-

ters on the mechanical properties of the materials that comprise the spheres, and the physical properties of the gasses that fluidize them, awaits more fundamental theory.

Finally, our new experimental data for the average value of  $T^*$  at the wall of a fluidized bed makes it possible to probe formulae derived from kinetic theory for the steady state of dense gasses: inertial pressure; inertial sound velocity; inertial viscosity; and inertial diffusion constant. Our experimental data for  $T^*$  implies that the simplest two phase model for the fluidization state neglects the dominant role of inertial forces strongly coupled to gas flow in the dense phase, and may need to be modified to include increasing gas flow through this phase with increasing gas superficial velocity.

### 22. List of symbols

$\boldsymbol{A}$	area of cylinder
a(f,0)	Fourier transform of acceleration at
	location $R_i = 0$ : $a(f) \equiv a(f,0)$
a(t)	time dependence of RMS acceleration
	(over band 10–20 kHz) during bed
_	collapse
$a^2$	mean squared acceleration over
	frequency band $f_1 \rightarrow f_2$ : $a^2 = \int_{f_1}^{f_2} S_a(f,0) df$
$a_{\rm n}^2$	mean squared noise over frequency
	band $f_1 \to f_2$ : $a_n^2 = \int_{f_1}^{f_2} S_n(f) df$
DIJ(4)	bed height as a function of time
BH(t)	vector velocity of particle
$C_{\rm e}$	extensional sound velocity of the
Ce	cylinder material
C*	inertial sound velocity of a dense hard
C	sphere gas held at a granular temperture
	of $T^*$ (Eqs. (35) and (36))
$e_{\mathrm{p}}$	coefficient of restitution for glass
Ψ	sphere
D	diameter of glass sphere
$\mathrm{d}E/\mathrm{d}t$	steady state power input into fixed bed
$D_{g}$	gas diffusion constant
$D_{ m g} D^*$	inertial diffusion constant of a dense
	hard sphere gas held at a granular
	temperture of $T^*$ (Eq. (39))
$D_{\mathrm{o}}$	diameter scaling constant
$F(f,R_i)$	Fourier transform of force at location
	$R_{i}$ : $a(f,0) = H(f,R_{i}) F(f,R_{i})$
F(r,t)	vector random force on particle in fluid
	bed
F(t)	dynamic force at wall for particle
	impact
$f(\boldsymbol{c}(\boldsymbol{r},t))$	velocity distribution function of particle
	at location, $r$ , and time, $t$

Fr	Froude number	II.	goe superficial valuative at angest of
Fr G		$U_{mb}$	gas superficial velocity at onset of
9	magnitude of $S_F(f)$ when it is	77	bubbling (minimum bubbling velocity)
G(A	independent of frequency	$U_{ m mf}$	gas superficial velocity at onset of
G(f)	ratio of $S_a^{Ar}(f,0)$ to $S_a^{He}(f,0)$		fluidization (minimum fluidization
g	gravitational constant (=9.8 m/s)	**	velocity)
$H(f,R_i)$	transfer function from force at $R_i$ to	$U_{\rm s}$	gas superficial velocity
_	accelerometer $R_i = 0$	$V(r,t) \equiv$	average particle velocity
$ H(f,R_i) ^2$	modulus squared of $H(f,R_i)$	$\langle c(\mathbf{r},t)\rangle$	
$<  H(f) ^2 >$	average of $ H(f,R_i) ^2$ over the area of	$v_{\mathbf{n}}$	RMS value of $v_n(\mathbf{r},t)$ where
	the cylinder containing the fluid bed		$v_{\rm n}^2 \equiv \langle v_{\rm n}(\mathbf{r},t)^2 \rangle$
	(Eq. (4a))	$v_{\rm n}(\boldsymbol{r},t)$	component of w normal to wall
h	wall thickness of the cylinder	w(r,t)	c(r,t)-V(r,t) = particle fluctuation
$I^2$	integral of $\langle  H(f) ^2 \rangle$ over frequency		velocity
	band	$V_{\mathrm{c}}$	bed collapse velocity = $\Delta BH/T_{\rm col}$
	f2	W	time interval for average of
	$f_1 \to f_2$ : $I^2 = \int_{f_1}^{f_2} \langle  H(f) ^2 \rangle df$		autocorrelation function
K	numerical constant in Eq. (11)	Greek letters	
	<del>-</del>		
$L_{ m mf}$	bed height at minimum fluidization	$\alpha$	cylinder damping constant
$L_{\rm s}$	bed height of packed bed of spheres	$\delta(t)$	Dirac delta function
	with diameter D and solids fraction	$\Delta P$	pressure drop across fluid bed
	$(1-\epsilon_{\rm s})$	$\Delta BH$	changes in bed height after bed collapse
m	particle mass	$\Delta (U_{\rm s}/U_{\rm mf})$	excess of $(v_n/U_s)(D/D_o)$ over Eq.
$<4m\rho_{\rm m}v_{\rm n}^3>$	weighed average of $4m\rho_{\rm m}v_{\rm n}^3$ over the		(15)
	cylinder with respect to $ H(f,R_i) ^2$	$\Delta A$	Differential wall area
(4)	(Eq. (4b))	$\Delta p$	momentum exchange with wall
p(t)	time dependence of plenum pressure in		$(2 mv_n)$
P*	bed collapse measurement	$\Delta P_{ m ke}$	pressure drop attributed to maintaining
P**	inertial or granular pressure of particles		particle kinetic energy constant
Ø.	(Eqs. (33) and (34))	$\Delta P_{ m visc}$	viscous pressure drop across fixed bed
P	time averaged power per unit volume		at minimum fluidization
	due to sphere/sphere and sphere/gas	$\epsilon_{ m mf}$	void fraction at minimum fluidization
0	interaction (Eq. (31))		velocity
Q	quality factor of the cylinder	$\epsilon_{ m s}$	void fraction in fluidized bed: $\rho_{\rm m} = \rho_{\rm o}$
	resonances: $\alpha = 1/Q$		$(1-\epsilon_{\rm s})$
<i>r</i>	vector location of particle	$\mu_{ m g}$	viscosity of fluidizing gas
R(f)	ratio of $S_a(f,0)$ to $\langle  H(f) ^2 \rangle$	$\mu^*$	inertial viscosity of a dense hard sphere
$S_{\rm a}(f,0)$	power spectrum of acceleration at		gas held at a granular temperature of
mAn(Ha) , and	$R_i = 0$ due to random particle impact		$T^*$ (Eqs. (37) and (38))
$S_{\rm a}^{\rm Ar(He)}(f,0)$	acceleration power spectrum of an	$\nu = \rho_{\rm b} v_{\rm n} \Delta A$	mean arrival rate of particles on wall
	accelerometer at $R = R_i$ for a bed		area $\Delta A$ , $\rho_{\rm b} v_{\rm n} \Delta A$
G (A	fluidized with argon (helium) gas	$ ho_{ m b}$	volume number density of particles
$S_{\mathbf{F}}(f)$	power spectrum of $F(t)$ for random		within fluid bed
	particle impact on area $\Delta A$	$ ho_{ m m}$	mass density of particles within fluid
$S_{\mathbf{F}}(f)$	power spectrum for $F(r,t)$		bed, $\rho_{\rm m} = m\rho_{\rm b}$
$S_{\rm n}(f)$	acceleration noise power spectrum	$ ho_{ m o}$	density of particle, $\rho_{\rm m} = \rho_{\rm o} (1 - \epsilon_{\rm s})$
$T^* \equiv$	granular temperature of particle	$\sigma$	Poisson ratio of the cylinder material
$(\langle w(r,t)^2 \rangle/3)$		$ au_{ m p}$	relaxation time of the sphere velocity
$T_{ m col}$	time for bed collapse	$\hat{oldsymbol{\Omega}}$	particle impact time with wall
$T_{ m g}$	time constant for gas leaving a fixed		
	bed		
$T_{ m I}$	mean time between sphere/sphere collisions	Acknowledgem	ents
$oldsymbol{ au}$		W/2 2m2	restability Dan Abalas for a suiting manifest
$T_{\rm o}$	exponential time constant of $a(t)$ in	we are very g	grateful to Ben Abeles for a critical reading

of an early version of this manuscript that greatly improved

bed collapse measurement

its clarity. We are grateful to Ping Sheng for pointing us toward the Maxwellian distribution and the granular temperature concept, and to Eric Herbolzheimer for general guidance in fluid dynamics. We would like to acknowledge early experiments on applying vibrational analysis to a laboratory scale fluidized bed by Dick Bellows and John Matsen. In the early stages of this research the mathematical rigor of Ben White was a valuable input into the credibility of the arguments leading to Eq. (2). We are grateful to John Matsen, Ron Rosensweig, Dick Bellows for stimulating discussions on fluid bed and transfer line phenomena; to Tom Witten of the University of Chicago, Rudi Klein of the University of Konstanz, Phil Pincus of UC Santa Barbara, and Roy Jackson of Princeton University for valuable conversations and encouragement; to George Walchuck for helping us to measure accurately gas flow; to Dee Redd, Arnie Kushnick, and Bill Varady for their valiant effort made to measure particle fluctuation velocity by fast video, frame grabbing and custom software to follow particle motion; to Wilton Gordon and Charles Chen for assistance in data acquisition and analysis of the relaxation phenomena; to Mike Pluchinsky for recommending and operating the NAC HSV-400 Color High Speed Video system for measurements of bed height during bed collapse.

#### References

- D. Kunii and O. Levenspiel, Fluidization Engineering, Krieger, Malabar, FL, 1987, p. 73.
- [2] A.M. Squires, M. Kwauk and A.A. Avidan, Science, 230 (1985) 1329.
- [3] R. Clift and J.R. Grace, in J.F. Davidson, R. Clift and D. Harrison (eds.), *Fluidization*, Academic Press, New York, 1985, pp. 73-128.
- [4] R. Jackson, in J.F. Davidson, R. Clift and D. Harrison (eds.), Fluidization, Academic Press, New York, 1985, pp. 47–72.
- [5] R. Jackson, in A.W. Weimer (ed.), Fluid Particle Technology, AIChE Symp. Ser. 301, Vol. 90, American Institute of Chemical Engineers, New York, 1994, pp. 1–30.
- [6] J.G. Yates and S.J.R. Simons, Int. J. Multiphase Flow, 20 (1994) 297.
- [7] G.K. Batchelor, J. Fluid Mech., 193 (1988) 75.
- [8] J.T. Jenkins and S.B. Savage, J. Fluid Mech., 155 (1983) 187.
- [9] P.K. Haff, J. Fluid Mech., 134 (1983) 401.
- [10] S.B. Savage, J. Fluid Mech., 194 (1988) 457.
- [11] T.G. Drake, J. Fluid Mech., 225 (1991) 121.
- [12] H.M. Jaeger and S.R. Nagel, Science, 255 (1992) 1523.
- [13] J. Ding and D. Gidaspow, AIChE J., 36 (1990) 523.
- [14] D.L. Koch, Phys. Fluids A, 2 (1990) 1711.
- [15] D. Gidaspow, Multiphase Flow and Fludization Continuum and Kinetic Theory Descriptions, Academic Press, San Diego, 1994, pp. 239–354.
- [16] J.T. Jenkins, in R.J. Knops and A.A. Lacey (eds.), Non-Classical Continuum Mechanics, Cambridge University Press, Cambridge, UK, 1987, pp. 213–225.
- [17] J.T. Jenkins and D.F. McTigue, in D.D. Joseph and D.G. Schaeffer (eds.), Two Phase Flow and Waves, Springer, New York, 1990, pp. 70-79.
- [18] E.J. Boyle, E.R. Gansley and W.A. Rogers, in W.G. Vogt and M.H. Mickle (eds.), *Modeling and Simulation Part 4, Proc. 20th Annu. Pittsburgh Conf.*, Instrument Society of America, Triangle Park, NC, 1989, pp. 1697–1708.
- [19] J.X. Bouillard, R.W. Lyczkowski, S. Folga, D. Gidaspow and G.F. Berry, Can. J. Chem. Eng., 67 (1989) 218.

- [20] J. Ding, R.W. Lyczkowski, S.W. Burge and D. Gidaspow, in A.W. Weimer (ed.), Fluidized Processes: Theory and Practice, AIChE Symp. Ser. 289, Vol. 88, American Institute of Chemical Engineers, New York, 1992, pp. 85–99.
- [21] D. Geldart, Powder Technol., 7 (1973) 285.
- [22] D. Geldart, in D. Geldart (ed.), Gas Fluidization Technology, Wiley, New York, 1986, pp. 11–51.
- [23] D. Geldart and L.S. Fan (eds.), in *Fluidization and Fluid Particle Systems*, AIChE Symp. Ser. 270, Vol. 85, American Institute of Chemical Engineers, New York, 1989, pp. 111-121.
- [24] J.R. Grace, in A.W. Weimer (ed.), Fluidized Processes, AIChE Symp. Ser. 289, Vol. 88, American Institute of Chemical Engineers, New York, 1992, pp. 1–16.
- [25] L. Chen and H. Weinstein, Chem. Eng. Sci., 49 (1993) 811.
- [26] D. ter Haar, Elements of Statistical Mechanicss, Rhinehart, New York, 1954, p. 468.
- [27] S.B. Savage and D.J. Jeffrey, J. Fluid Mech., 110 (1981) 255.
- [28] D. Gidaspow, R. Bezburuah and J. Ding, in O.E. Potter and D.J. Nicklin (eds.), Fluidization VII, Proc. 7th Engineering Foundation Conf. Fluidization, Brisbane, Australia, May 1992, Engineering Foundation, New York, 1992, pp. 75–82.
- [29] C.S. Campbell, Annu. Rev. Fluid Mech., 22 (1990) 57.
- [30] Y. Tsuji, Y. Morikawa and H. Shiomi, J. Fluid Mech., 139 (1984) 417.
- [31] M. Yianneskis, Powder Technol., 49 (1987) 261.
- [32] M.Y. Louge, S.A. Iyer, E.P. Giannelis, D.J. Lischer and H. Chang, Applied Optics, 30 (1991) 1976.
- [33] J. Militzer, J.P. Hebb, G. Jollimore and K. Shakourzadeh, in O.E. Potter and D.J. Nicklin (eds.), Fluidization VII, Proc. 7th Engineering Foundation Conf. Fluidization, Brisbane, Australia, May 1992, Engineering Foundation, New York, 1992, pp. 763-766.
- [34] A. van der Ziel, in T. Kailath (ed.), Noise: Sources, Characterization, Measurement, Prentice Hall, Englewood Cliffs, NJ, 1970, pp. 9, 169.
- [35] D.E. Newland, An Introduction to Random Vibrations and Spectral and Wavelet Analysis, Longman Scientific/Wiley, New York, 3rd edn., 1993, p. 477.
- [36] L.D. Landau and E.M. Lifshitz, Theory of Elasticity, Pergamon, Oxford, 2nd edn., 1970, p. 36.
- [37] C.S. Campbell and D.G. Wang, Meas. Sci. Technol., 1 (1990) 1279.
- [38] C.S. Daw et al., Phys. Rev. Lett., 75 (1995) 2308.
- [39] A.N. Norris, (1996) to be published.
- [40] L. Ye, G. Cody, M. Zhou, P. Sheng and A. Norris, Phys. Rev. Lett., 69 (1992) 3080.
- [41] G. Cody, L. Ye, M. Zhou, P. Sheng and A. Norris, in C.M. Soukoulis (ed.), *Photonic Band Gaps and Localization*, Plenum, New York, 1993, pp. 339–353.
- [42] N.I. Gelperin and V.G. Einstein, in J.F. Davidson and D. Harrison (eds.), Fluidization, Academic Press, New York, 1971, pp. 541-567.
- [43] S.C. Tsinontides and R. Jackson, J. Fluid Mech., 255 (1993) 237.
- [44] N.A. Fuchs, The Mechanics of Aerosols, Dover, New York, 1989, pp. 308, 338.
- [45] R.R. Rathbone, M. Ghadiri and R. Clift, in J.R. Grace, L.W. Schemilt and M.A. Bergougnou (eds.), *Fluidization VI, Proc. Int. Conf. Fluidization, Banff, Canada, May 1989*, Engineering Foundation, New York, 1989, pp. 629-635.
- [46] R.S. Brodkey, The Phenomena of Fluid Motions, Addison-Wesley, Reading, MA, 1967, p. 164.
- [47] J.X. Bouillard and D. Gidaspow, Powder Technol., 68 (1991) 13.
- [48] R.J. Kubo, in S.F. Edwards (ed.), Repr. Ser. Reports on Progress in Physics: Many Body Problems, Benjamin, New York, 1969, pp. 235– 284.
- [49] G.E. Uhlenbeck and L.S. Ornstein, Phys. Rev., 36 (1930) 823.
- [50] M.C. Wang and G.E. Uhlenbeck, Rev. Mod. Phys., 17 (1945) 322.
- [51] K.L. Johnson, Contact Mechanics, Cambridge University Press, Cambridge, 1986, p. 353.
- [52] S.F. Foerster, M.Y. Louge, H. Chang and K. Allia, Phys. Fluids, 6 (1994) 1108.

- [53] J.M. Pendlebury, Kinetic Theory, Adam Hilger, Boston, MA, 1985, p.
- [54] C.S. Campbell and D.G. Wang, J. Fluid Mech., 227 (1991) 468.
- [55] C.S. Campbell and K. Rahman, Meas. Sci. Tech., 3 (1992) 702.
- [56] W. Polashenski, Jr. and J.C. Chen, *Powder Technol.*, (1995) to be published.
- [57] P.H. Calderbank and F.D. Toor, in J.F. Davidson and D. Harrison (eds.), Fluidization, Academic Press, New York, 1971, pp. 383-427.
- [58] J.F. Davidson, in E. Guazzelli and L. Oger (eds.), Mobile Particulate Systems, Kluwer, Dordrecht, The Netherlands, 1995, pp. 173–220.
- [59] R. Ocone and G. Astarita, J. Rheology, 38 (1994) 129.
- [60] D. Musmarra, S. Vaccaro, M. Filla and L. Massimilla, Int. J. Multiphase Flow, 19 (1993) 705.
- [61] R. Roy, J.F. Davidson and V.G. Tuponogov, Chem. Eng. Sci., 45 (1990) 3233.

- [62] L. Gibilaro, P. Foscolo and R. di Felice, in D.D. Joseph and D.G. Schaeffer (eds.), Two Phase Flow and Waves, Springer, New York, 1990, pp. 56-69.
- [63] D. Gidaspow, Y.P. Tsuo and K.M. Luo, in J.R. Grace, L.W. Schemilt and M.A. Bergougnou (eds.), Fluidization VI, Proc. Int. Conf. Fluidization, Banff, Canada, May 1989, Engineering Foundation, New York, 1989, pp. 81–89.
- [64] J. Furukawa and T. Ohmae, Ind. Eng. Chem., 50 (1958) 828.
- [65] K. Schugerl, in J.F. Davidson and D. Harrison (eds.), Fluidization, Academic Press, New York, 1971, pp. 261–291.
- [66] D. Gidaspow and L. Huillin, Collisional Viscosity of FCC Particles in a CFB, AIChE Annu. Meet., Miami Beach, FL, 1995.
- [67] O. Zik and J. Stavans, Europhys. Lett., 16 (1991) 258.
- [68] O. Zik, J. Stavans and Y. Rabin, Europhys. Lett., 17 (1991) 319.
- [69] R.W. Clift, in A. Weimer (ed.), Fluid Bed Processes, AIChE Symp. Ser. 289, Vol. 89, American Institute of Chemical Engineers, New York, 1993, pp. 1-17.